ΔNTcf4 was kindly provided by H. Clevers (Utrecht, The Netherlands).

Plasmid Constructs. The sequences of the human and mouse LECT2 genes have already been described.[19,20] The human and mouse promoters were synthesized from human and mouse genomic DNA by polymerase chain reaction (PCR) cloning.[19] *In situ* hybridization (ISH) probes were prepared from full-length human LECT2 cDNA (gi: 4504976) cloned in the *Sma*I site of pSP72 (Promega). Riboprobes were synthesized from linearized *Bgl*II (sense) and *Xho*I (antisense) plasmid. GS riboprobes were generated as previously described.[21]

Northern Blotting. Total RNA was extracted from frozen liver using the guanidium thiocyanate single-step procedure; an aliquot (15 μg) was electrophoresed through 1% agarose-6% formaldehyde gel. The RNA samples were transferred to Hybond N+ (Amersham Pharmacia) membranes and hybridized with the corresponding ^{32}P-labeled probes.

Western Blotting. Tissues were homogenized in Laemmli buffer (1:10 wt/vol). Total proteins (10 μg) were separated using 10% sodium dodecyl sulfate-polyacrylamide gel electrophoresis (SDS-PAGE), and were transferred to a nitrocellulose membrane. LECT2 was detected using polyclonal anti-mouse LECT2.[22] The signals were visualized using the chemiluminescence detection system.

Radioactive* In Situ *Hybridization. The radioactive ISH detection of messenger RNA sequences has been extensively described previously.[21] The LECT2 probes (both orientations) were double-labeled. Slides were exposed for 7 days for GS and 21 days for LECT2.

Chemotactic Assay. *N*-formyl-methionyl-leucyl-phenylalanine (fMLP) was purchased from Sigma (St Louis, MO). Stock solutions were stored in DMSO at −20°C. Recombinant mouse and human LECT2 proteins were produced from CHO cells as previously described.[22] Random and directed migration of PMN was studied using the Boyden chamber technique.[23] Suspensions of 0.5 × 10^6 PMN in 100 μL HBSS containing 1% BSA were incubated in the upper compartment of a chamber separated from the lower compartment by a cellulose filter (3 μm diameter pores; Millipore, Bedford, MA). The lower compartment contained various concentrations of LECT2 or fMLP. In some experiments, the chemoattractant was placed in the PMN chamber to destroy the chemotactic gradient. Chambers were incubated at 37°C for 40 minutes in 95% humidified air; filters were treated with ethanol and stained with hemalum. Unstimulated and directed migrations of PMN were measured as the migration front (at least 10 PMN) under a microscope. Five fields were analyzed for each filter. Results, obtained from 3 experiments, are expressed in micrometers.

Immunohistochemistry. Immunohistochemistry was undertaken using 5 μm sections of formalin-fixed, paraffin-embedded liver. Sections were incubated with specific antibodies for 1 hour. The primary antibodies used were polyclonal anti-mouse LECT2,[20] monoclonal anti-GS (1/200; BD Transduction Laboratories, Lexington, KY), monoclonal anti–β-catenin (1/500; BD Transduction Laboratories) polyclonal anti-GFP (1/50; BD Biosciences), and polyclonal antihemagglutinin (1/400; Clontech: Roche, Basel, Switzerland). LECT2, GS, β-catenin, GFP, and hemagglutinin (HA) were visualized using an immunoperoxidase protocol (Vectastain ABC Kit; Vector, Burlingame, CA). The proliferation marker Ki67 was detected immunohistochemically as previously described.[14]

Real-Time Reverse-Transcriptase (RT)-PCR Analysis. Two μg of total RNA was reverse transcribed in a final volume of 40 μL as previously described.[14]

PCR reactions were undertaken using the LightCycler Instrument (Roche Molecular Biochemicals) and the LightCycler FastStart DNA Master Sybr Green I Reagent Kit (Roche Molecular Biochemicals), according to the manufacturer's protocol. PCR was run in 10 μL total volume (2 μL of diluted cDNA corresponding to 5 ng of total RNA and 8 μL of reaction mix containing 1 μL of 10 μmol of each primer) for 45 cycles. For each tumor sample, 2 reactions, 1 for the target gene and 1 for the reference 18S ribosome RNA, were undertaken in separate capillaries.

Quantification was undertaken using the calibrator-normalized Relative Quantification Software. The relative target gene expression was normalized on the basis of its 18S ribosomal content and to a calibrator which was normal human liver. The calibrator was included in each run and its normalized gene expression was set at a value 1. For each tumoral liver sample, the relative gene expression was expressed as x-fold the realtive expression of the calibrator. Primer sequences were: human LECT2 gene lectF: 5′-GGCAAGTCTTCCAATGA-3′, LectR: 5′CACATGCGATTGTATGC-3′, human GS gene GSF: 5′AAGTGTGTGGAAGAGTTGCC-3′, GSR: 5′-TGC TCACCATGTCCATTATC-3′, 18S gene: 18SF: 5′-GTAACCCGTTGAACCCCATT-3′, 18SR: 5′-CCA TCCAATCGGTAGTAGCG.

Results

Identification of LECT2 Gene by SSH. We used SSH to identify early target genes regulated by Wnt/β-catenin signaling. The livers of mice injected with an ad-

enovirus that encodes for an oncogenic form of β-catenin (AdβcatS37A, HA-tagged) or with control adenoviruses that encode for LacZ or GFP (AdLacZ and AdGFP) were removed 48 hours postinjection and the RNA extracted. The resulting subtracted cDNA library was screened. We isolated four genes that are strongly expressed: the GS gene that we had previously isolated as a hepatic β-catenin target gene,[15] CYP2E1, RNase A family 4, and the LECT2 gene (data not shown). We focused on the LECT2 gene, because our recent results of studies of transgenic mice that lack the LECT2 gene suggested that LECT2 may regulate the homeostasis of natural killer T cells in the liver and may be involved in the pathogenesis of hepatitis LECT2 expression was substantially increased in the livers of mice that had been injected with AdβcatS37A (Fig. 1A). The early expression of LECT2 in response to activated β-catenin was also confirmed in an independent experiment. Livers were obtained from mice that had been sacrificed after injection of AdβcatS37A or control AdGFP. The LECT2 signal began to increase 24 hours after injection and reached a peak at 48 hours; it then remained almost stable for up to 120 hours in AdβcatS37A-infected livers (Fig.1B).

The distribution of LECT2 protein in mouse liver has not been published previously. Immunohistochemical studies showed that LECT2 expression is restricted to the perivenous hepatocytes in normal mouse liver (Fig. 2C). However, LECT2 expression was found throughout the liver lobules of AdβcatS37A-infected mice; the distribution of oncogenic β-catenin, as revealed by HA immunohistochemistry, was similar. Activation of the Wnt pathway was revealed by HA cytosolic and nuclear staining (Fig. 1C). Thus, the targeted activation of the Wnt pathway in hepatocytes induces LECT2 expression in these cells. In contrast, no induction of LECT2 expression was observed in AdGFP-infected livers, even though the livers were infected to about the same extent, as judged by GFP and HA staining (Fig. 1C).

Up-regulation of LECT2 Expression Is Linked to an Activation of β-Catenin Signaling in the Liver. Northern and Western blot analyses demonstrated that LECT2 gene expression is more strongly increased in the liver of ΔN131β-catenin transgenic mice than in the liver of a nontransgenic mouse (wild type; Figs. 2A and B). As expected, LECT2 expression was found throughout the liver lobule where oncogenic β-catenin was present (Fig. 2C).

We also studied L-PK/c-myc mice with liver tumors: more than 50% of the tumors had activating mutations in the β-catenin gene.[3] Our earlier studies of such mice showed that activation of β-catenin signaling in liver tumors was associated with the overexpression of the gene

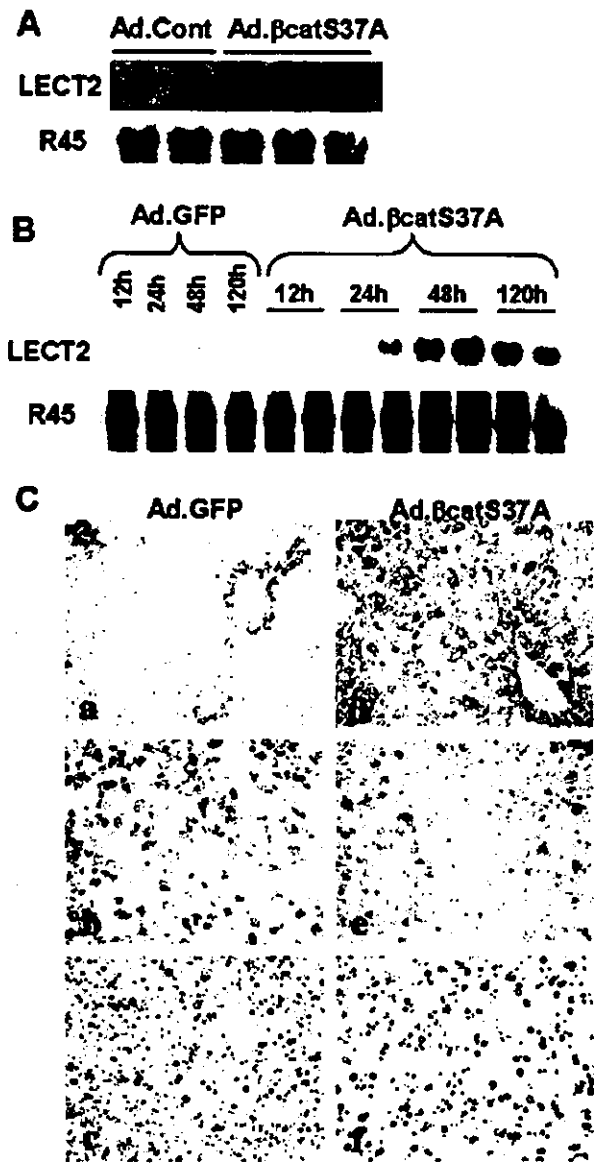

Fig. 1. Identification of LECT2 as a potential β-catenin target gene in infected liver of mice. (A) LECT2 gene expression in adenovirus-infected livers used for the SSH library. RNA samples from livers of mice used for the SSH library, infected with recombinant adenoviruses that encoded for GFP, *Lac Z* (Ad.Cont), or an activated β-catenin (Ad.βcatS37A) were evaluated by Northern blotting. Blots were standardized with ribosomal probe R45. (B) LECT2 gene expression in adenovirus-infected livers. Mice were injected with the indicated adenoviruses and sacrificed 12, 24, 48, or 120 hours after injection (2 mice for each time point). RNA from infected livers was evaluated by Northern blotting. (C) Distribution of LECT2 in adenovirus-infected livers. (a and d) Sections of liver infected with adenoviruses for 120 hours were assessed for distribution of LECT2, (b and e) transgene expression, and (c and f) proliferation by KI-67 immunohistochemical staining. Transgene expression was assessed using (b) GFP immunohistochemical staining and (e) HA immunohistochemical staining that visualized HA-tagged β-catenin S37A. Activation of β-catenin signaling was revealed by cytosolic and nuclear HA immunohistochemical staining. (a, b, and c) Livers infected with adenoviruses encoding GFP (Ad.GFP) for 120 hours. (Magnification, ×200). (d, e, and f) Livers infected by AdβcatS37A for 120 hours.

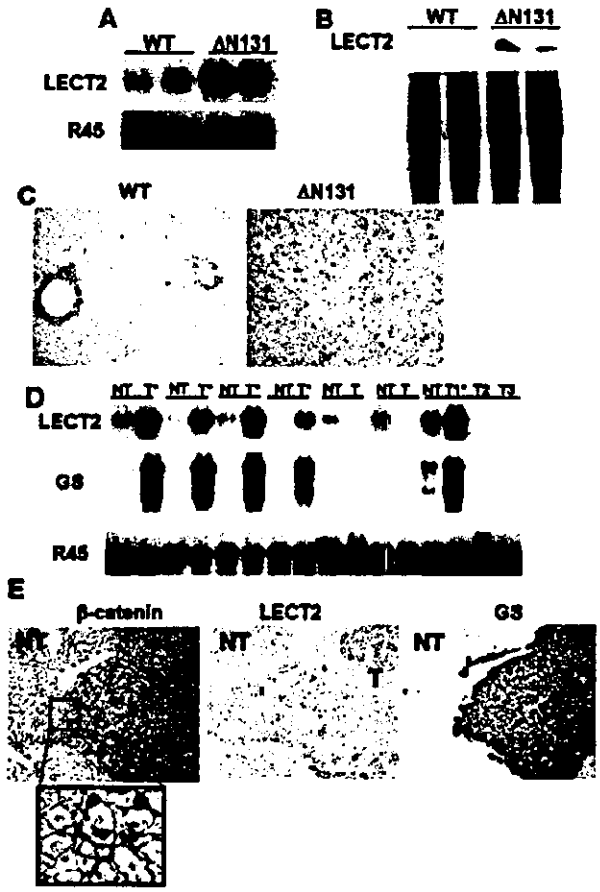

Fig. 2. LECT2 and GS gene expression in the livers of ΔN131β-catenin and PK/c-myc transgenic mice. (A) LECT2 gene expression in ΔN131β-catenin transgenic mice. RNA samples from the liver of wild type (WT) and ΔN131β-catenin transgenic (ΔN131) mice were evaluated by Northern blotting. Blots were standardized using ribosomal probe R45. (B) Western blot analysis of livers from ΔN131β-catenin transgenic mice. Total cell extracts were analyzed using SDS-PAGE and immunoblotted with anti-LECT2 antibody. (C) Sections of the livers of WT and ΔN131β-catenin (ΔN131) mice were stained with an anti-LECT2 antibody. (Magnification, ×200.) (D) Northern blot analysis of RNA from liver tumor tissue (T, T1, T2, T3) from PK/c-myc transgenic mice and nontumor liver (NT). The asterisk (*) marks tumors with activated β-catenin. (E) Immunohistochemical detection of β-catenin, LECT2, and GS in liver tumors from PK/c-myc mice. (**Left**) a representative tumor nodule (T) showing cytosolic and nuclear staining for β-catenin that was not present in nontumor tissue (NT). (**Middle**) Immunohistochemical detection of LECT2 showing uniform staining for LECT2 in the tumor (T). The adjacent nontumoral tissue (NT) exhibits perivenous staining for LECT2. (**Right**) Section with uniform GS staining throughout the tumor (T) and perivenous GS staining in the adjacent nontumor tissue (NT). (Magnification, ×200.) This illustration is representative of 15 liver tumors analyzed.

that encodes for GS.[15] Accordingly, we assayed LECT2 and GS gene expressions in isolated hepatic tumor nodules—with or without activated β-catenin—and compared their expression to that in adjacent nontumor tissue. The expression of LECT2 gene was up-regulated in the tumors associated with activated β-catenin and GS expression. The liver tumors that were negative for GS were also negative for LECT2 (Fig. 2D). Immunohistochemistry revealed that expression of LECT2 was restricted to the perivenous region of nontumor tissue. Both LECT2 and GS were widely distributed throughout tumor tissue in which there was activation of β-catenin signaling, as indicated by positive immunohistochemical staining for β-catenin in the cytosol and, occasionally, in the nucleus (Fig. 2E).

To confirm that the up-regulation of LECT2 expression was associated with activation of β-catenin signaling in the liver, we analyzed the expression of LECT2 in liver tumors that developed in ASV transgenic mice following the expression of SV40 early sequences.[16] The Wnt pathway is not activated in the tumors of such mice[24]. No up-regulation of LECT2 was observed in liver tumors of ASV transgenic mice, although these tumors were highly proliferative (Figs. 3B, C, and D). Absence of induction of LECT2 expression in this model was confirmed by Northern blot analysis (data not shown). We also found no increased LECT2 expression in AdGFP-infected mice, although there was substantial hepatocellular proliferation in this model (Fig. 1C).

LECT2 Is a Downstream Target of the β-Catenin/TCF-4 Signaling Pathway. The identification of several LEF/TCF binding sequences in the mouse and human

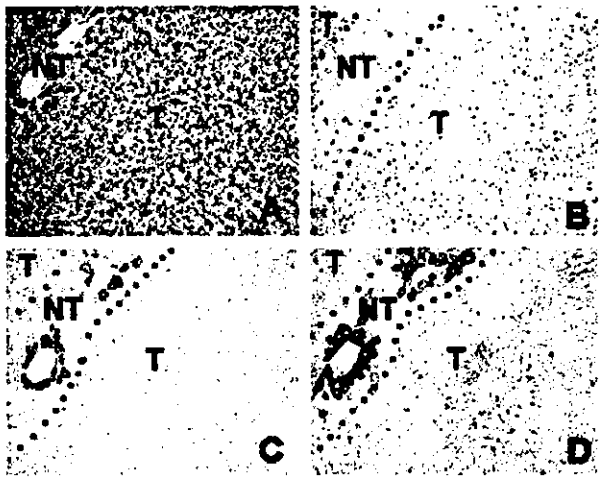

Fig. 3. Distribution of LECT2 and GS in liver tumors from SV40 large T-antigen transgenic mice. Immunohistochemical detection of Ki67, LECT2, and GS in liver tumor of SV40 large T-antigen transgenic mice (ASV). (A) Histology, hematoxylin-eosin staining. (B) Ki67 staining showing hepatocyte proliferation in tumor tissue (T) and no staining in the adjacent nontumor tissue (NT). (C) Immunohistochemical detection of LECT2. There is perivenous LECT2 staining in the nontumor tissue (NT), no staining for LECT2 in the tumor (T). (D) Immunohistochemical detection of GS. GS staining was similar to that for LECT2: it was restricted to the perivenous region of the nontumoral tissue. (Magnification, ×200.) This illustration is representative of the results obtained from 3 different ASV mice.

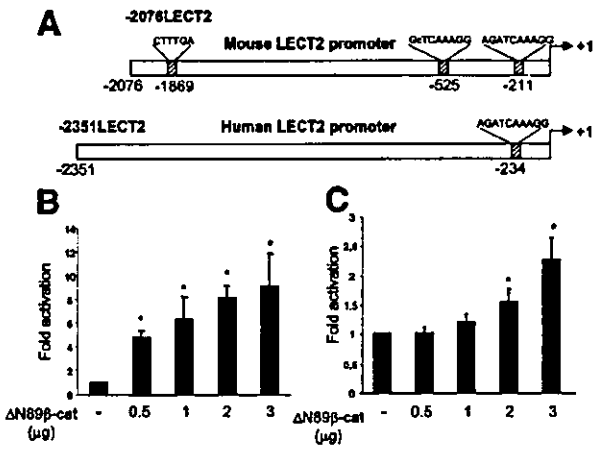

Fig. 4. The mouse and human LECT2 promoters are activated by β-catenin. (A) Diagram showing the mouse LECT2 promoter (−2076LECT2) and the human LECT2 promoter (−2351LECT2). Putative LEF/TCF binding sites are located from the ATG site; the proximal LEF/TCF binding site matched to the consensus LEF/TCF site. It is the same in both the mouse and human LECT2 promoter. (B) Huh7 cells were transfected with 0.1 μg of mouse LECT2 promoter (−2076LECT2-LUC) together with increasing concentrations of activated β-catenin: 0, 0.5, 1, 2, and 3 μg of ΔN89β-catenin-encoding plasmid (ΔN89β-cat). Results are presented as x-fold induction relative to transfection of the reporter by an empty expression vector. The **bars** represent the mean values of 3 experiments, each undertaken in duplicate. **Error bars** represent SEMs. $*P < .05$. (C) Huh7 cells were transfected with 1 μg of human promoter (−2351hLECT2) together with 0, 0.5, 1, 2, and 3 μg of ΔN89β-cat. Results are presented as x-fold induction relative to transfection of the reporter by an empty expression vector. The **bars** represent the mean values of 3 experiments, each undertaken in duplicate. **Error bars** represent SEMs. $*P < .05$.

LECT2 promoters (Fig. 4A) led us to determine whether the LECT2 promoter was a direct transcriptional target for activation by β-catenin. To this end, we used Huh7 and HepG2 hepatoma cell lines which differ in their β-catenin status; Huh7 and HepG2 are wild type and activated mutant, respectively.[3]

The induction of both mouse and human LECT2 promoter activities by β-catenin was demonstrated by transient cotransfection studies in Huh7 cells using promoter-luciferase reporter constructs containing about 2 kbp of 5′-flanking regulatory region of the mouse and human LECT2 genes and an oncogenic ββ-catenin construct (ΔN89β-catenin). The result was a significant dose-dependent increase in the mouse and human promoter activities in response to activated β-catenin. The mouse promoter was activated up to 10-fold (Figs. 4B and C). The effect was strongly inhibited by cotransfection with a dominant-negative TCF-4 expression construct (ΔNTCF4) that prevented transactivation through the LEF/TCF recognition motifs (Fig. 5A). The cotransfection of the ΔNTCF4 expression vector in HepG2 cells, which ex-

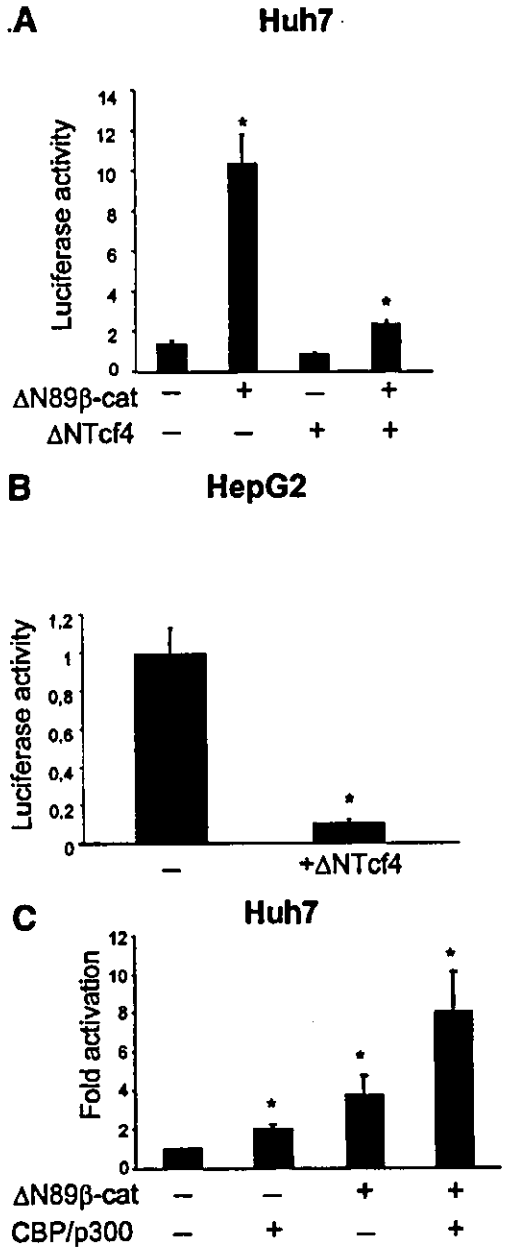

Fig. 5. Control of LECT2 promoter activity by β-catenin: involvement of LEF/TCF sites and the CBP/p300 coactivator. (A)Huh7 cells were transfected with 0.1 μg of mouse LECT2 promoter and 1 μg of β-catenin or empty vector, and 1 μg of ΔNTCF4 expression vector or empty vector. Data are expressed as normalized luciferase activity relative to Renilla control. (B) HepG2 cells were transfected with 0.1 μg of mouse LECT2 promoter and 1 μg of ΔNTCF4 or empty expression vector. Data are expressed as normalized luciferase activity relative to Renilla control. (C) LECT2 promoter transactivation by the CBP/p300 coactivator. Huh7 cells were transfected with 0.1 μg of mouse LECT2 promoter and 0.5 μg of ΔN89β-cat or empty vector, plus 1.5 μg of CBP/p300 or empty vector. Results are presented as x-fold induction relative to transfection of the reporter by empty expression vector. **Bars** represent the means of 3 independent duplicates, each undertaken in duplicates. **Error bars** represent the SD. $*P < .05$.

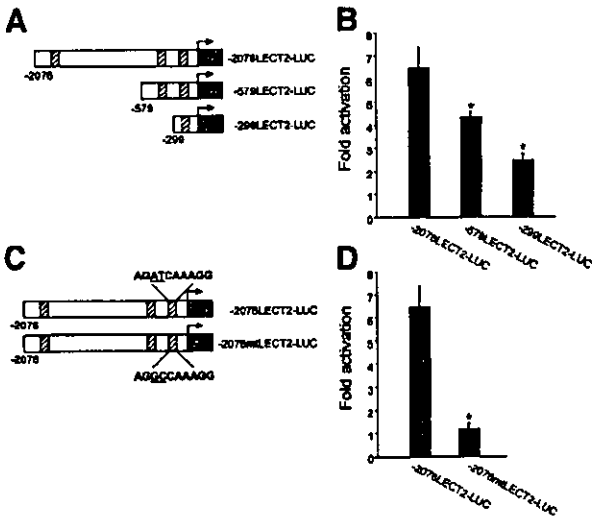

Fig. 6. Role of the proximal LEF/TCF binding sequence of the LECT2 promoter in β-catenin-mediated transactivation (A) Deletion constructs of the mouse LECT2 promoter (−579LECT2-LUC and −299LECT2-LUC) in the pGL3 luciferase reporter plasmid. (B) The deletion constructs of the mouse LECT2 promoter (0.1 μg) were transfected into Huh7 cells as shown in Fig. 5C. (C) The mutated mouse LECT2 reporter construct showing the AT to GC change at nucleotides −209 and −208 (−2076mtLECT2-LUC). D) Huh7 cells were transfected with the wild type or mutated mouse LECT2 reporter construct (0.1 μg) as described in Fig. 5C. Transfections were carried out in triplicate, each undertaken in duplicate. Data are means ± SD. $^*P < .05$.

press an endogenous activated β-catenin, reduced substanially the activity of the LECT2 promoter induced by β-catenin (Fig. 5B). Thus, β-catenin/TCF transactivation controls the activity of the LECT2 promoter. Since the coactivators CBPand p300 have been shown to activate β-catenin/TCF transcription of some Wnt-responsive genes,[25] they could cooperate with β-catenin to activate LECT2 promoter. Transfection with CBP/p300 more than doubled the LECT2 promoter activity induced by β-catenin, whereas the CBP/p300 expression construct alone had little effect on the LECT2 promoter in the absence of β-catenin (Fig. 5C).

Analysis of the mouse promoter shows that it contains 3 potential LEF/TCF binding sequences. To identify the sequences in the LECT2 promoter that can confer transactivation by β-catenin, 2 deletion constructs were generated (Fig. 6A). Analysis of these deletion constructs revealed a progressive decrease of the transactivation induced by β-catenin (Fig. 6B). The smallest construct, which contained only the proximal LEF/TCF site, still mediated a 2- to 3-fold induction of LECT2 promoter activity. This finding indicates that the proximal site could be important in cooperation with distal sites for the transactivation of mouse LECT2 promoter by β-catenin. The proximal LEF/TCF site matched perfectly to the consensus sequence and is conserved in the human LECT2 promoter (Fig. 4A). Thus, this site appears to be a good candidate to support the transcriptional activity of LECT2 promoter by β-catenin. We tested this hypothesis by introducing point mutations in the LEF/TCF proximal site in the full-length LECT2 promoter (−2076mtLECT2-LUC; Fig. 6C). Mutation of the proximal LEF/TCF binding site completely abolished transactivation of the LECT2 promoter by β-catenin (Fig. 6D).

LECT2 is therefore a direct transcriptional target of β-catenin.

Chemotactic Properties of LECT2. The LECT2 protein was initially purified from the culture fluid of phytohemagglutinin-activated human T-cell leukemia SKW-3 cells as a possible chemotactic factor for human neutrophils.[26]

To further characterize the chemotactic property of LECT2, we used a recombinant LECT2 protein produced from CHO cells[22] and tested its chemotactic properties using human PMN. The chemotactic activity of LECT2 was compared to that of the tripeptide fMLP, which is a potent neutrophil chemoattractant.[18,27] LECT2 induced a bell-shaped migration pattern as a function of its concentration; this finding is characteristic of a chemotactic ligand (Fig. 7). Significant directed migration was observed in the presence of 10 to 25 nM LECT2, whereas at a high concentration (50 nmol) LECT2 was inactive, presumably because of chemotactic desensitization of PMN. fMLP induced more directed migration over a wider active concentration range than LECT2. To determine whether the stimulated migration induced by LECT2 may be mediated by chemokinetic activity of PMN, we abolished the chemotactic gradient by titrating LECT2 or fMLP into the cell compartment of the Boyden chamber. Under these conditions, the directed PMN migration was completely prevented (data not shown). This finding confirms that LECT2 is a chemoattractant for human neutrophils.

Expression of the LECT2 Gene in Human Liver Tumors. To investigate if LECT2 could be implicated in human liver cancer, we analyzed LECT2 gene expression using real-time RT-PCR of liver tumors in which the Wnt pathway is frequently altered. We first quantified the relative degree of RNA expression of LECT2 and GS in 18 human HCC samples, in which there were activated mutations of the β-catenin gene. As expected, all these tumors exhibited a high degree of GS expression.[15] In contrast, LECT2 expression was up-regulated in only 5 of these tumors (Fig. 8). Analysis of 33 HCC samples that did not display β-catenin mutations indicated up-regulation of LECT2 in only 6 samples. Interestingly, all of the

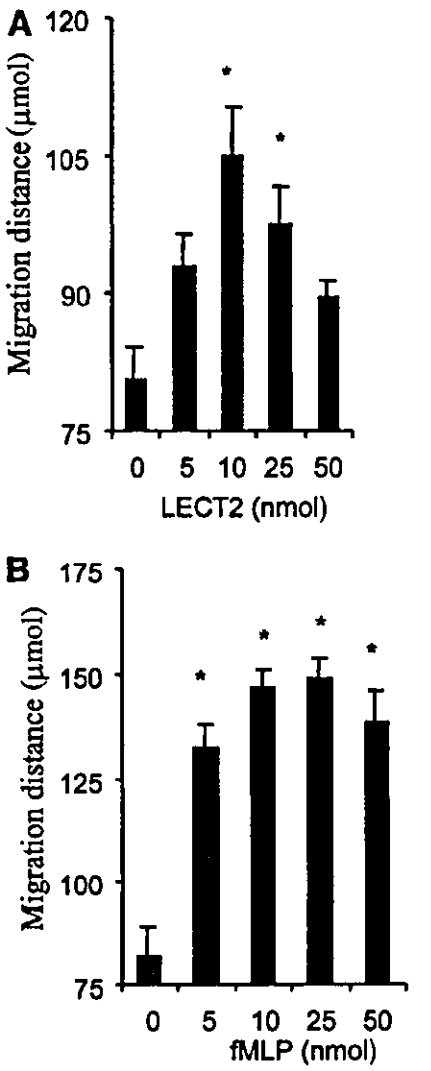

Fig. 7. PMN chemotactic activity of LECT2 and fMLP. The migration of PMN was measured in the presence or absence of various concentrations of (A) LECT2 or (B) fMLP placed in the lower compartment of the Boyden chamber. Results represent the migration front expressed in micrometers (mean ± SEM of 5 individual fields for each concentration, from a representative experiment). The significance of differences between data obtained from 3 independent experiments with random and stimulated migrations were determined using Student's *t* test. $^*P < .05$.

6 LECT2-positive HCC samples were also positive for GS, suggesting that these samples may have mutations of another partner of the Wnt pathway (Fig. 8). Altogether, these results indicated that even though LECT2 was generally down-regulated in human HCC samples, LECT2 was up-regulated only in a subset of human HCC, a subset in which the Wnt pathway was altered. We also analyzed hepatoblastoma samples; deregulation of the Wnt pathway occurs in more than 90% of these tumors[4] We analyszed LECT2 expression in 14 samples using real-time RT-PCR. A high level of LECT2 expression was observed in 13 samples. Overexpression of GS was substantial in all of the samples tested (Fig. 8). ISH, used to localize LECT2 expression, confirmed that LECT2 was up-regulated in hepatoblastomas. LECT2 was detected in the tumor areas that exhibited activation of β-catenin signaling associated with GS expression (Fig. 9).

Discussion

The Wnt pathway is frequently deregulated in carcinogenesis. Considerable effort is currently being made to identify the downstream β-catenin target genes; those that have been identified may be important for understanding the role of Wnt signaling in carcinogenesis because they are involved in cell proliferation, survival, differentiation, and migration.[10,11] However, it has become clear that the Wnt response is tissue-specific. Ex-

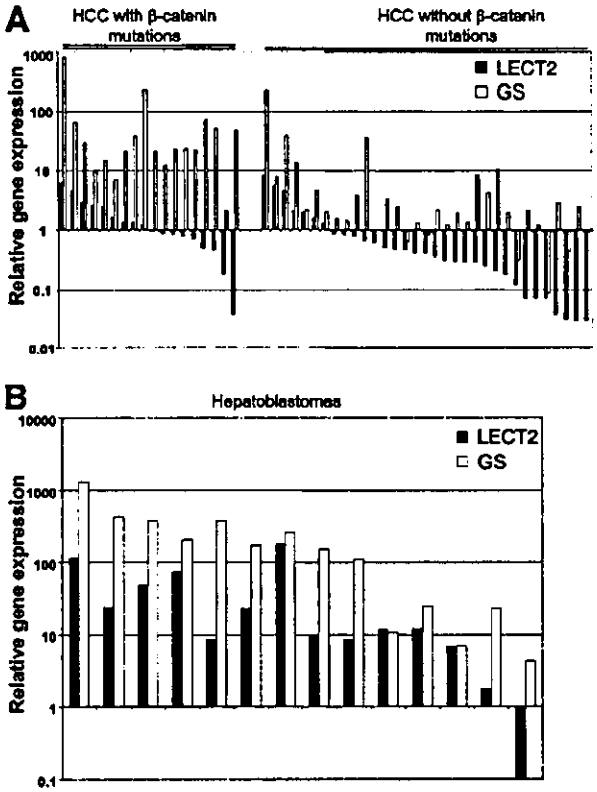

Fig. 8. Up-regulation of LECT2 in human liver tumors Histograms on a logarithmic scale showing the relative expression of LECT2 and GS genes measured in (A) a panel of hepatocellular carcinomas (HCC) with β-catenin mutations and a panel of HCC that have no activating mutations of β-catenin, and (B) in a panel of hepatoblastomas. Relative gene expression was determined using real-time RT-PCR, as described in Materials and Methods, and was expressed as fold difference relative to normal liver, after normalization of each measurement to 18S ribosomal RNA.

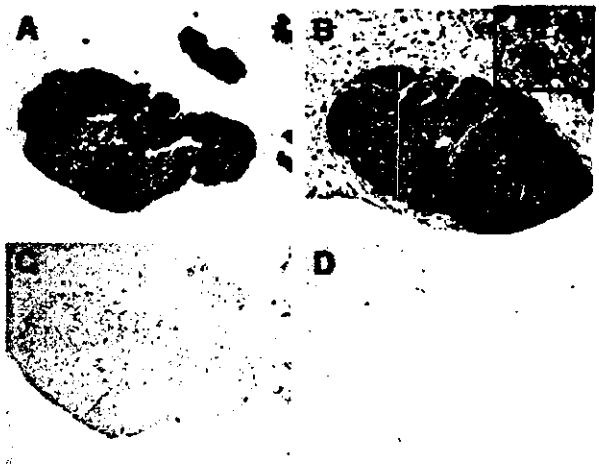

Fig. 9. Expression of LECT2, GS, and β-catenin in hepatoblastoma by *in situ* hybridization. Representative *in situ* hybridization of [^{35}S]-labeled probes for (A) GS antisense, (C) LECT2 antisense, and (D)LECT2 sense in serial sections of a single hepatoblastoma. This illustration is representative of 11 cases analyzed. (Magnification, ×40.) (B) Immunohistochemical staining of β-catenin. Note the tumor area displayed activated β-catenin signaling, as revealed by cytosolic and nuclear accumulation of β-catenin, that parallels the signals of LECT2 and GS. (Magnification, ×40.) (**Insert**) β-catenin cytosolic and nuclear accumulation. (Magnification, ×400.)

pression of activated β-catenin is sufficient to induce polyposis in the intestine[28,29] but is not sufficient to induce hepatocarcinogenesis in the liver. We and others have observed substantial hepatomegaly in response to activation of β-catenin signaling in the liver, but other genetic events are likely to be required for hepatic tumorigenesis.[14,30] Therefore, it is important to identify the target genes of β-catenin in the liver. We used an adenovirus-mediated expression of activated β-catenin to isolate early target genes. We identified the LECT2 gene as a direct target of β-catenin signaling in the liver.

We found that LECT2 promoter activity is increased considerably by activation of β-catenin, and is blocked by a dominant-negative form of TCF-4. We have also identified the LEF/TCF site as being crucial for a response to β-catenin. Our studies in mice with activated β-catenin showed that β-catenin signaling strongly induced LECT2 expression in hepatocytes. As LECT2 is mainly expressed in the liver, we assessed whether LECT2 could be a liver-specific response of the Wnt pathway. We analyzed LECT2 expression in another tumor in which activation of the Wnt pathway is frequent: colon cancer. We observed no induction of LECT2 expression in intestinal epithelial cells of polyps that develop in a mouse model of colon cancer that we recently developed (Colnot et al., unpublished manuscript). Such mice have a new germline mutation of the *Apc* gene and a high level of activation of β-catenin signaling, as indicated by cytosolic and nuclear staining of β-catenin in all epithelial cells of their polyps. So far, few β-catenin target genes have been isolated from liver.[15,31] LECT2 can be induced by β-catenin in the liver but not in the intestine, and it may be an important target relating to the tissue-specific response of the Wnt pathway in hepatic tissue.

Interestingly, LECT2 gene expression is confined to a well-defined pericentral compartment, consisting of 1 to 2 layers of hepatocytes in the normal mouse liver; this expression is similar to that of 3 other hepatic β-catenin-induced genes linked to glutamine metabolism that we identified previously.[15] The zonation of the liver lobule is determined during development of the liver; the molecular mechanisms involved are not known. From our results, it is tempting to speculate that the Wnt pathway in the liver may participate in the establishment of zonation.

The relevance of LECT2 in human liver carcinogenesis has been addressed by examining the level of expression of LECT2 in human liver tumors. We found substantial induction of LECT2 in most of the hepatoblastomas studied; in this tumor, activation of the Wnt pathway is frequent.[4] In contrast, an up-regulation of LECT2 was found only in a subset of HCCs associated with activation of the Wnt pathway. However, LECT2 expression was generally decreased in human HCCs in accordance with previously published findings.[32,33] Hepatoblastoma and HCC are 2 primary liver tumors that differ with respect to their histological manifestations and genetic changes. HCC is a heterogeneous tumor associated with multiple genetic changes; only a limited number of chromosomal changes have been found in hepatoblastomas.[4] The loss of LECT2 expression in HCCs that have aberrant β-catenin signaling could result from "cross-talking" with one or more other signaling pathways induced by different genetic changes that may occurr during tumor progression. At present, the role of LECT2 in liver carcinogenesis is unknown. LECT2 was first isolated as a possible chemotactic factor for neutrophils.[26] Using recombinant protein, we have further characterized the chemotactic property of LECT2 for human neutrophils *in vitro*. We searched for leukocyte infiltration in tumors that overexpressed LECT2, such as those associated with L-PK/c-myc, but we did not find any evidence of an inflammatory process in such tumors. Two hypotheses may be proposed: (1) leukocyte infiltration may be a transient event that cannot be observed in the tumor, and (2) the role of LECT2 in liver carcinogenesis may be linked to another function of LECT2. The study of transgenic mice lacking the LECT2 gene revealed that the role of LECT2 is related to the homeostasis of NKT cells in the liver; LECT2 may modulate the inflammatory and immune response

induced by the development of the tumor. Since HCC develops most commonly in patients with chronic hepatitis or cirrhosis induced by viral or inflammatory factors, understanding the role of LECT2 in liver carcinogenesis is of interest and may lead to new therapeutic perspectives.

Acknowledgment: We thank Professor Axel Kahn for strong support and for critically reading the manuscript, and all the members of our team for helpful discussion. We also thank M. A. Buendia (Institut Pasteur, France) for providing HCC and hepatoblastoma RNA samples, Professor Benoit Terris (Hôpital Cochin, Service d'Anatomopathologie) for providing frozen HCC samples, J. Kitajewski (Columbia University, NY) for providing the recombinant adenoviruses, F. Letourneur and N. Lebrun (Institut Cochin) for sequencing, and Dr. Owen Parkes for editing the manuscript.

References

1. Bosch FX, Ribes J, Borras J. Epidemiology of primary liver cancer. Semin Liver Dis 1999;19:271–285.
2. Buendia MA. Genetics of hepatocellular carcinoma. Semin Cancer Biol 2000;10:185–200.
3. de La Coste A, Romagnolo B, Billuart P, Renard CA, Buendia MA, Soubrane O, et al. Somatic mutations of the beta-catenin gene are frequent in mouse and human hepatocellular carcinomas. Proc Natl Acad Sci USA 1998;95:8847–8851.
4. Buendia MA. Genetic alterations in hepatoblastoma and hepatocellular carcinoma: common and distinctive aspects. Med Pediatr Oncol 2002;39: 530–535.
5. Laurent-Puig P, Legoix P, Bluteau O, Belghiti J, Franco D, Binot F, et al. Genetic alterations associated with hepatocellular carcinomas define distinct pathways of hepatocarcinogenesis. Gastroenterology 2001;120:1763–1773.
6. Wei Y, Fabre M, Branchereau S, Gauthier F, Perilongo G, Buendia MA. Activation of beta-catenin in epithelial and mesenchymal hepatoblastomas. Oncogene 2000;19:498–504.
7. Koch A, Denkhaus D, Albrecht S, Leuschner I, von Schweinitz D, Pietsch T. Childhood hepatoblastomas frequently carry a mutated degradation. Cancer Res 1999;59:269–273.
8. Satoh S, Daigo Y, Furukawa Y, Kato T, Miwa N, Nishiwaki T, et al. AXIN1 mutations in hepatocellular carcinomas, and growth suppression in cancer cells by virus-mediated transfer of AXIN1. Nat Genet 2000;24: 245–250.
9. Taniguchi K, Roberts LR, Aderca IN, Dong X, Qian C, Murphy LM, et al. Mutational spectrum of beta-catenin, AXIN1, and AXIN2 in hepatocellular carcinomas and hepatoblastomas. Oncogene 2002;21:4863–4871.
10. Polakis P. Wnt signaling and cancer. Genes Dev 2000;14:1837–1851.
11. Giles RH, van Es JH, Clevers H. Caught up in a Wnt storm: Wnt signaling in cancer. Biochim Biophys Acta 2003;1653:1–24.
12. He TC, Sparks AB, Rago C, Hermeking H, Zawel L, da Costa LT, et al. Identification of c-MYC as a target of the APC pathway. Science 1998; 281:1509–1512.
13. Tetsu O, McCormick F. Beta-catenin regulates expression of cyclin D1 in colon carcinoma cells. Nature 1999;398:422–426.
14. Cadoret A, Ovejero C, Saadi-Kheddouci S, Souil E, Fabre M, Romagnolo B, et al. Hepatomegaly in transgenic mice expressing an oncogenic form of beta- catenin. Cancer Res 2001;61:3245–3249.
15. Cadoret A, Ovejero C, Terris B, Souil E, Levy L, Lamers WH, et al. New targets of beta-catenin signaling in the liver are involved in the glutamine metabolism. Oncogene 2002;21:8293–8301.
16. Bennoun M, Grimber G, Couton D, Seye A, Molina T, Briand P, et al. The amino-terminal region of SV40 large T antigen is sufficient to induce hepatic tumours in mice. Oncogene 1998;17:1253–1259.
17. Young CS, Kitamura M, Hardy S, Kitajewski J. Wnt-1 induces growth, cytosolic beta-catenin, and Tcf/Lef transcriptional activation in Rat-1 fibroblasts. Mol Cell Biol 1998;18:2474–2485.
18. Perianin A, Pedruzzi E, Hakim J. W-7, a calmodulin antagonist, primes the stimulation of human neutrophil respiratory burst by formyl peptides and platelet-activating factor. FEBS Lett 1994;342:135–138.
19. Yamagoe S, Kameoka Y, Hashimoto K, Mizuno S, Suzuki K. Molecular cloning, structural characterization, and chromosomal mapping of the human LECT2 gene. Genomics 1998;48:324–329.
20. Yamagoe S, Mizuno S, Suzuki K. Molecular cloning of human and bovine LECT2 having a neutrophil chemotactic activity and its specific expression in the liver. Biochim Biophys Acta 1998;1396:105–113.
21. Moorman AF, Houweling AC, de Boer PA, Christoffels VM. Sensitive nonradioactive detection of mRNA in tissue sections: novel application of the whole-mount in situ hybridization protocol. J Histochem Cytochem 2001;49:1–8.
22. Yamagoe S, Akasaka T, Uchida T, Hachiya T, Okabe T, Yamakawa Y, et al. Expression of a neutrophil chemotactic protein LECT2 in human hepatocytes revealed by immunochemical studies using polyclonal and monoclonal antibodies to a recombinant LECT2. Biochem Biophys Res Commun 1997;237:116–120.
23. Boyden S. The chemotactic effect of mixture of antibody and antigen on polymorphonuclear leukocytes. J Exp Med 1962;115:453–466.
24. Umeda T, Yamamoto T, Kajino K, Hino O. beta-catenin mutations are absent in hepatocellular carcinomas of SV40 T-antigen transgenic mice. Int J Oncol 2000;16:1133–1136.
25. Hecht A, Vleminckx K, Stemmler MP, van Roy F, Kemler R. The p300/CBP acetyltransferases function as transcriptional coactivators of beta-catenin in vertebrates. EMBO J 2000;19:1839–1850.
26. Yamagoe S, Yamakawa Y, Matsuo Y, Minowada J, Mizuno S, Suzuki K. Purification and primary amino acid sequence of a novel neutrophil chemotactic factor LECT2. Immunol Lett 1996;52:9–13.
27. Chenoweth DE, Rowe JG, Hugli TE. A modified method for chemotaxis under agarose. J Immunol Methods 1979;25:337–353.
28. Romagnolo B, Berrebi D, Saadi-Keddoucci S, Porteu A, Pichard AL, Peuchmaur M, et al. Intestinal dysplasia and adenoma in transgenic mice after overexpression of an activated beta-catenin. Cancer Res 1999;59:3875–3879.
29. Harada N, Tamai Y, Ishikawa T, Sauer B, Takaku K, Oshima M, et al. Intestinal polyposis in mice with a dominant stable mutation of the beta-catenin gene. EMBO J 1999;18:5931–5942.
30. Harada N, Miyoshi H, Murai N, Oshima H, Tamai Y, Oshima M, et al. Lack of tumorigenesis in the mouse liver after adenovirus-mediated expression of a dominant stable mutant of beta-catenin. Cancer Res 2002;62: 1971–1977.
31. Levy L, Neuveut C, Renard CA, Charneau P, Branchereau S, Gauthier F, et al. Transcriptional activation of interleukin-8 by beta-catenin-Tcf4. J Biol Chem 2002;277:42386–42393.
32. Uchida T, Nagai H, Gotoh K, Kanagawa H, Kouyama H, Kawanishi T, et al. Expression pattern of a newly recognized protein, LECT2, in hepatocellular carcinoma and its premalignant lesion. Pathol Int 1999;49:147–151.
33. Okabe H, Satoh S, Kato T, Kitahara O, Yanagawa R, Yamaoka Y, et al. Genome-wide analysis of gene expression in human hepatocellular carcinomas using cDNA microarray: identification of genes involved in viral carcinogenesis and tumor progression. Cancer Res 2001;61:2129–2137.

Increase in Hepatic NKT Cells in Leukocyte Cell-Derived Chemotaxin 2-Deficient Mice Contributes to Severe Concanavalin A-Induced Hepatitis[1]

Takeshi Saito,* Akinori Okumura,* Hisami Watanabe,† Masahide Asano,[2‡] Akiko Ishida-Okawara,* Junko Sakagami,‡ Katsuko Sudo,‡ Yoshimi Hatano-Yokoe,§ Jelena S. Bezbradica,¶ Sebastian Joyce,¶ Toru Abo,‖ Yoichiro Iwakura,‡ Kazuo Suzuki,* and Satoshi Yamagoe[3]*

Leukocyte cell-derived chemotaxin 2 (LECT2) was originally identified for its possible chemotactic activity against human neutrophils in vitro. It is a 16-kDa protein that is preferentially expressed in the liver. Its homologues have been widely identified in many vertebrates. Current evidence suggests that LECT2 may be a multifunctional protein like cytokines. However, the function of LECT2 in vivo remains unclear. To elucidate the role of this protein in vivo, we have generated LECT2-deficient ($LECT2^{-/-}$) mice. We found that the proportion of NKT cells in the liver increased significantly in $LECT2^{-/-}$ mice, although those of conventional T cells, NK cells, and other cell types were comparable with those in wild-type mice. Consistent with increased hepatic NKT cell number, the production of IL-4 and IFN-γ was augmented in $LECT2^{-/-}$ mice upon stimulation with α-galactosylceramide, which specifically activates Vα14 NKT cells. In addition, NKT cell-mediated cytotoxic activity against syngeneic thymocytes increased in hepatic mononuclear cells obtained from $LECT2^{-/-}$ mice in vitro. Interestingly, the hepatic injury was exacerbated in $LECT2^{-/-}$ mice upon treatment with Con A, possibly because of the significantly higher expression of IL-4 and Fas ligand. These results suggest that LECT2 might regulate the homeostasis of NKT cells in the liver and might be involved in the pathogenesis of hepatitis. *The Journal of Immunology,* **2004, 173: 579–585.**

Leukocyte cell-derived chemotaxin 2 (LECT2)[4] was originally identified from the culture fluid of the human T cell line SKW-3 in the process of screening for a novel neutrophil chemotactic protein (1). LECT2 is expressed preferentially in the liver in a constitutive manner. LECT2 protein is secreted into the bloodstream (2, 3). Proteins homologous to LECT2 have been isolated in many vertebrates (4, 5). LECT2 is identical with chondromodulin II, which was identified as a growth stimulator for chondrocytes and osteoblasts (6). The polymorphism of human LECT2 at $Val^{58}Ile$ is associated with the severity of rheumatoid arthritis in the Japanese population (7). We recently reported that the expression of mouse LECT2 was transiently decreased during Con A-induced hepatitis, an experimental model for human autoimmune hepatitis that is induced by the expression of cytokines and cytotoxic molecules associated with effects from other immune cells, such as $CD4^+$ T lymphocytes and macrophages (8). Thus, LECT2 seems to be a multifunctional protein like cytokines. However, the function of LECT2 in vivo remains unclear.

NKT cells form a distinctive T cell subpopulation that has some of the characteristics of NK cells. NKT cells are present in various lymphoid organs and are especially abundant in the liver (9–11). In mice, NKT cells commonly express a semi-invariant TCR and NK1.1 Ag, and their development and functions are regulated by CD1d (9, 12). There is growing evidence that NKT cells play an important role in immune responses (9–13). It is well established that NKT cells express large amounts of cytokines, especially IFN-γ and IL-4, and their functional disorders are characteristic of various diseases (9, 12, 13). Recently, some groups reported that NKT cells played an essential role in Con A-induced hepatitis (14–16).

In this study we generated $LECT2^{-/-}$ mice with the aim of clearly identifying the role of LECT2 in vivo. We found that these mice showed an increased number of hepatic NKT cells, which appeared to function as they do in wild-type mice. To examine the biological effect of this phenotype, we used a Con A-induced hepatitis model. The deficiency of LECT2 led to severe liver injury, possibly because of excessive expression of IL-4 and Fas ligand (FasL) by the increase in the number of hepatic NKT cells.

Materials and Methods

Mice

Wild-type C57BL/6J (B6) mice purchased from CLEA Japan were housed at the National Institute of Infectious Diseases. Mice used in this study

*Department of Bioactive Molecules, National Institute of Infectious Diseases, Tokyo, Japan; †Division of Cellular and Molecular Immunology, Center of Molecular Biosciences, University of Ryukyus, Okinawa, Japan; ‡Center for Experimental Medicine, Institute of Medical Science, University of Tokyo, Tokyo, Japan; §Department of Internal Medicine, Showa University, Tokyo, Japan; ¶Department of Microbiology and Immunology, Vanderbilt University School of Medicine, Nashville, TN 37232; and ‖Department of Immunology, Niigata University School of Medicine, Niigata, Japan

Received for publication October 16, 2003. Accepted for publication April 28, 2004.

The costs of publication of this article were defrayed in part by the payment of page charges. This article must therefore be hereby marked *advertisement* in accordance with 18 U.S.C. Section 1734 solely to indicate this fact.

[1] This work was supported by grants from the Japan Health Sciences Foundation; the Ministry of Health, Labor, and Welfare of Japan; the Ministry of Education, Culture, Sports, Science, and Technology of Japan; and National Institutes of Health Grant AI42284.

[2] Current address: Division of Transgenic Animal Science, Advanced Science Research Center, Kanazawa University, Kanazawa 920-8640, Japan.

[3] Address correspondence and reprint requests to Dr. Satoshi Yamagoe, Department of Bioactive Molecules, National Institute of Infectious Diseases, 1-23-1 Toyama, Shinjuku-ku, Tokyo 162-8640, Japan. E-mail address: syamagoe@nih.go.jp

[4] Abbreviations used in this paper: LECT2, leukocyte cell-derived chemotaxin 2; FasL, Fas ligand; α-GalCer, α-galactosylceramide; GPT, glutamic pyruvic transaminase; MNC, mononuclear cell.

0022-1767/04/$02.00

were maintained under specific pathogen-free conditions and were usually used at 8–12 wk of age according to the guidelines of the National Institute of Infectious Diseases animal care and use committee.

Generation of LECT2$^{-/-}$ mice

To construct the targeting vector (pKO-9), two fragments (5′ end, 7.7 kb; 3′ end, 1.4 kb) of the genomic DNA flanking the coding region of the 129-derived *lect2* gene (17) were subcloned between the *Bam*HI and *Spe*I sites and between the *Aat*I and *Sca*I sites of the pBluescript II KS$^+$ vector (Stratagene, La Jolla, CA), respectively. The pGKneobpA cassette (18) was inserted between *Spe*I and *Aat*I for positive selection (Fig. 1*A*). The DT-A cassette (19) was ligated at the 5′ end of the targeting vector for negative selection. E14.1 ES cells (1×10^7 cells) were transferred with the linearized targeting vector by electroporation and were selected with G418 (Invitrogen, Carlsbad, CA). Homologous recombinants were screened by PCR and confirmed by Southern blot hybridization (Fig. 1*A*; data not shown). The forward primer (P2) in the pGKneobpA cassette was 5′-GGTGGATGTG GAATGTGTGC-3′, and the reverse primer (P5) outside the targeting vector was 5′-ACCATCTACTAGCTCTTGTAG-3′. Chimeric mice were generated by the aggregation method (19) with some modifications. The chimeras were mated with B6 mice, and homozygous mutant mice were generated by the intercrossing of heterozygotes. LECT2$^{-/-}$ mice and littermates were genotyped by PCR (Fig. 1*B*). The primer sequences used were as follows: LECT2-common, 5′-CCACCCCACCTAAGATGTATGCTGC-3′; LECT2-wild-type, 5′-CCAGGATTCTAATGTCGTCCTTGTTGG-3′; and LECT2-knockout, 5′-CCTTCTTGACGAGTTCTTCTGAGGGG-3′.

Immunoblot analysis

Two micrograms of serum prepared from LECT2$^{-/-}$ mice and their littermates was resolved by SDS-PAGE (4–20%) and transferred to Immobilon-P (Millipore, Bedford, MA). The blots were incubated with rabbit anti-mouse LECT2 against a recombinant mouse LECT2 produced stably by CHO cells. The immunoreactive protein was visualized using an ECL kit (Amersham Pharmacia Biotech, Piscataway, NJ).

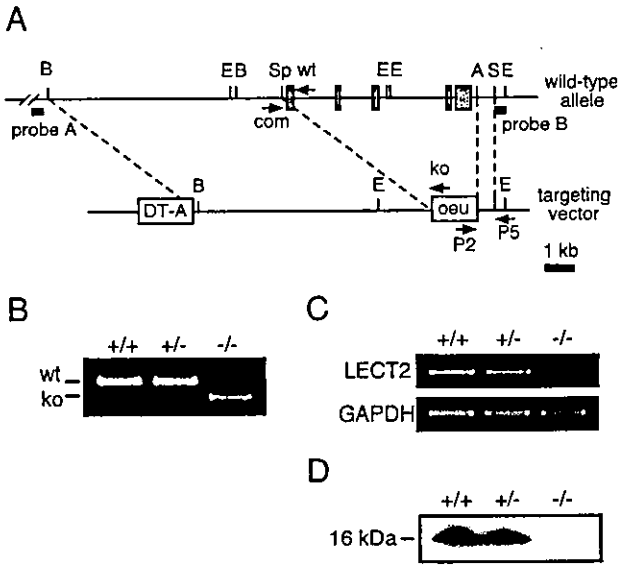

FIGURE 1. Generation of LECT2$^{-/-}$ mice. *A*, Endogenous *Lect2* gene and targeting vector. A 6.4-kb *Spe*I-*Aat*I fragment containing all exons for LECT2 was replaced with pGKneobpA. A, *Aat*I; B, *Bam*HI; E, *Eco*RI; S, *Sca*I; Sp, *Spe*I. Arrows indicate primers for genotyping. Probes A and B were used to confirm the correct recombination by Southern blot analysis. PCR primer LECT2-common (com), LECT2-wild type (wt), and LECT2-knockout (ko) were used for genotyping. *B*, Genotyping of LECT2$^{-/-}$ mice and littermates. Genomic DNA from embryonic stem cells or mouse tails were analyzed by PCR. This analysis yields 517- and 385-bp bands for the wild-type and targeted alleles, respectively. *C*, Total liver RNAs were reverse transcribed and subjected to PCR analysis. The primers used are described in *Materials and Methods*. *D*, Serum from mice was analyzed by Western blot analysis using rabbit anti-LECT2 polyclonal Ab (2).

Lymphocyte preparations

Mice anesthetized with ether were killed by exsanguination via the axillary artery. The liver and spleen were then removed. Hepatic mononuclear cells (MNCs) were prepared as described previously (20). Briefly, the liver lobes were minced to small pieces, pressed through 200-gauge stainless steel mesh, and suspended in Eagle's MEM (Sigma-Aldrich, St. Louis, MO) supplemented with 5 mM HEPES (pH 7.5) and 2% FBS. After washing, the pellet was resuspended in 35% Percoll solution (Amersham Pharmacia Biotech) containing heparin (100 U/ml) and centrifuged at 2000 rpm for 15 min. The pellet was then resuspended in RBC lysis solution (155 mM NH_4Cl, 10 mM $KHCO_3$, 1 mM EDTA, and 17 mM Tris, pH 7.3) and washed twice with MEM. Splenocytes were prepared by forcing minced spleens through stainless steel mesh and were used after RBC lysis.

Flow cytometric analysis

Single-cell suspensions from the liver and spleen were incubated with mAbs against cell surface markers (BD Pharmingen, San Diego, CA). PE-labeled CD1d-α-galactosylceramide (CD1d-α-GalCer) tetramer (21) and FITC-, PE-, allophycocyanin-, or PerCP-conjugated Abs specific for murine CD3 (145-2C11), CD4 (RM4-5), NK1.1 (PK136), Gr-1 (RB6-8C5), Mac-1 (M1/70), and FasL (MFL-3) were used for flow cytometric analyses. Apoptotic cells were stained with an Annexin V-FITC Apoptosis Detection I kit (BD Pharmingen) and then analyzed with FACSCalibur using CellQuest software (BD Biosciences, San Jose, CA).

Administration of α-GalCer

α-GalCer was kindly provided by Kirin Brewery (Gunma, Japan). This reagent was dissolved in 0.5% polysorbate 20 (Nikko Chemical, Tokyo, Japan) at a concentration of 200 μg/ml, then further diluted with physiological saline. For in vivo administration, α-GalCer was injected i.p. at a dose of 100 μg/kg body weight. For in vitro stimulation of MNCs, α-GalCer was added to the culture medium (RPMI 1640 supplemented with 2% FBS) at a concentration of 100 ng/ml.

Cytotoxicity assays

The cytotoxicity assays were performed by a method previously described (22). Briefly, YAC-1 cells and B6 thymocytes for target cells were labeled with sodium [^{51}Cr]chromate (Amersham Pharmacia Biotech) for 2 h and washed three times with RPMI 1640. Effector cells were serially diluted and mixed with ^{51}Cr-labeled target cells ($1–2 \times 10^4$ cells) in a U-bottom, 96-well microculture plate. The plates were centrifuged and incubated for 4 h at 37°C. At the end of the culture, 100 μl of the supernatant was determined by adding RPMI 1640. Maximum release was determined by adding 1 M HCl. The percentage of specific release was calculated as [(experimental release − spontaneous release)/(maximum release − spontaneous release)] × 100.

Con A-induced liver injury

Male B6 (wild-type controls) and LECT2$^{-/-}$ B6 mice were injected i.v. with 25 mg/kg Con A (type IV; Sigma-Aldrich). Two, 5, and 8 h after Con A injection, sera were collected to measure the level of cytokines and glutamic pyruvic transaminase (GPT) activity, and liver tissue was removed to detect the cytokine mRNAs and for immunohistochemical analysis.

Cytokine and transaminase measurement

The levels of serum IFN-γ, TNF-α, and IL-4 were quantified using an OptEIA ELISA set (BD Pharmingen). Serum GPT activity was measured with a Transaminase CII-test Wako kit (Wako Pure Chemical, Osaka, Japan).

Histology and TUNEL staining

Liver tissues were fixed in 4% neutralized formalin and embedded in paraffin, then sliced to a thickness of 3 μm. For histological examination, sections were stained with H&E. Apoptotic cells were detected with TUNEL staining using an In Situ Cell Death Detection Kit, POD (Roche, Mannheim, Germany).

Semiquantitative RT-PCR

The total liver RNA for each mouse was isolated using Isogen reagent (Wako Pure Chemical). One microgram of RNA was reverse transcribed with a ReverTra Ace (Toyobo, Osaka, Japan) to obtain cDNA. The primer sequences used in PCR were as follows: LECT2, 5′-ACGTGTGACAGC TATGGCTGTGGACAG-3′ and 5′-AGGTATGCTGTGGGGTCACTGGAG

TC-3′; and GAPDH, 5′-CCCCTGGCCAAGGTCATCCATGACAACTTT-3′ and 5′-GGCCATGAGGTCCACCACCCTGTTGCTGTA-3′. Reactions were conducted under the following conditions: precycling at 94°C for 1 min, then 25 cycles consisting of denaturation at 94°C for 30 s, annealing at 55°C for 30 s, and polymerization at 72°C for 1 min.

Quantitative real-time RT-PCR

Quantitative real-time RT-PCR was performed using ABI PRISM 7000 Sequence Detection System (Applied Biosystems, Foster City, CA) according to the manufacturer's protocol. Primers and TaqMan probes specific for TNF-α, IL-4, and FasL were obtained from Assay-on-Demand Gene Expression Products (Applied Biosystems), and IFN-γ was derived from TaqMan Pre-Developed Assay Reagents (Applied Biosystems). For endogenous control, the level of GAPDH in each sample was assayed using TaqMan Rodent GAPDH Control Reagents VIC (Applied Biosystems). Data analyses were performed on ABI PRISM 7000 SDS software version 1.0 (Applied Biosystems).

Statistical analysis

Results were expressed as the mean ± SD. Statistical analyses were conducted using Student's t test or the Mann-Whitney U test. A value of $p < 0.05$ was considered significant.

Results

Generation of LECT2$^{-/-}$ mice

To delete the *lect2* gene, a targeting construct carrying a neomycin cassette was placed within the *lect2* locus in such a way that all exons for this gene were deleted (Fig. 1*A*). Correct targeting of the *lect2* locus was confirmed by PCR and genomic Southern blot analysis (Fig. 1*B*; data not shown). LECT2$^{+/-}$ mice were backcrossed for 10 generations to B6 and intercrossed to generate LECT2$^{-/-}$ mice. Complete loss of LECT2 expression in the liver and serum of LECT2$^{-/-}$ mice was confirmed by RT-PCR and immunoblot analysis, respectively (Fig. 1, *C* and *D*). LECT2$^{-/-}$ mice were born at the Mendelian ratio and were indistinguishable in appearance from wild-type mice. Both male and female LECT2$^{-/-}$ mice were fertile.

Flow cytometric analysis of MNCs from LECT2$^{-/-}$ and wild-type mice

LECT2 is preferentially expressed in the liver (2). LECT2$^{-/-}$ mice exhibited no obvious abnormality in the size or histology of the liver or in serum GPT activity. In addition, the sizes of other tissues, such as spleen and thymus, were normal. We recently reported a possible additional role of LECT2 in Con A-induced hepatic injury (3). Con A-induced hepatitis results from injuries inflicted by various immune cells such as CD4$^+$ T cells and NK1.1$^+$ T cells (8, 14–16). Therefore, we measured the proportions of immune cells in the liver by flow cytometric analysis. Interestingly, we observed that the percentage of hepatic CD3^{int} NK1.1$^+$ cells in LECT2$^{-/-}$ mice was significantly higher than that in wild-

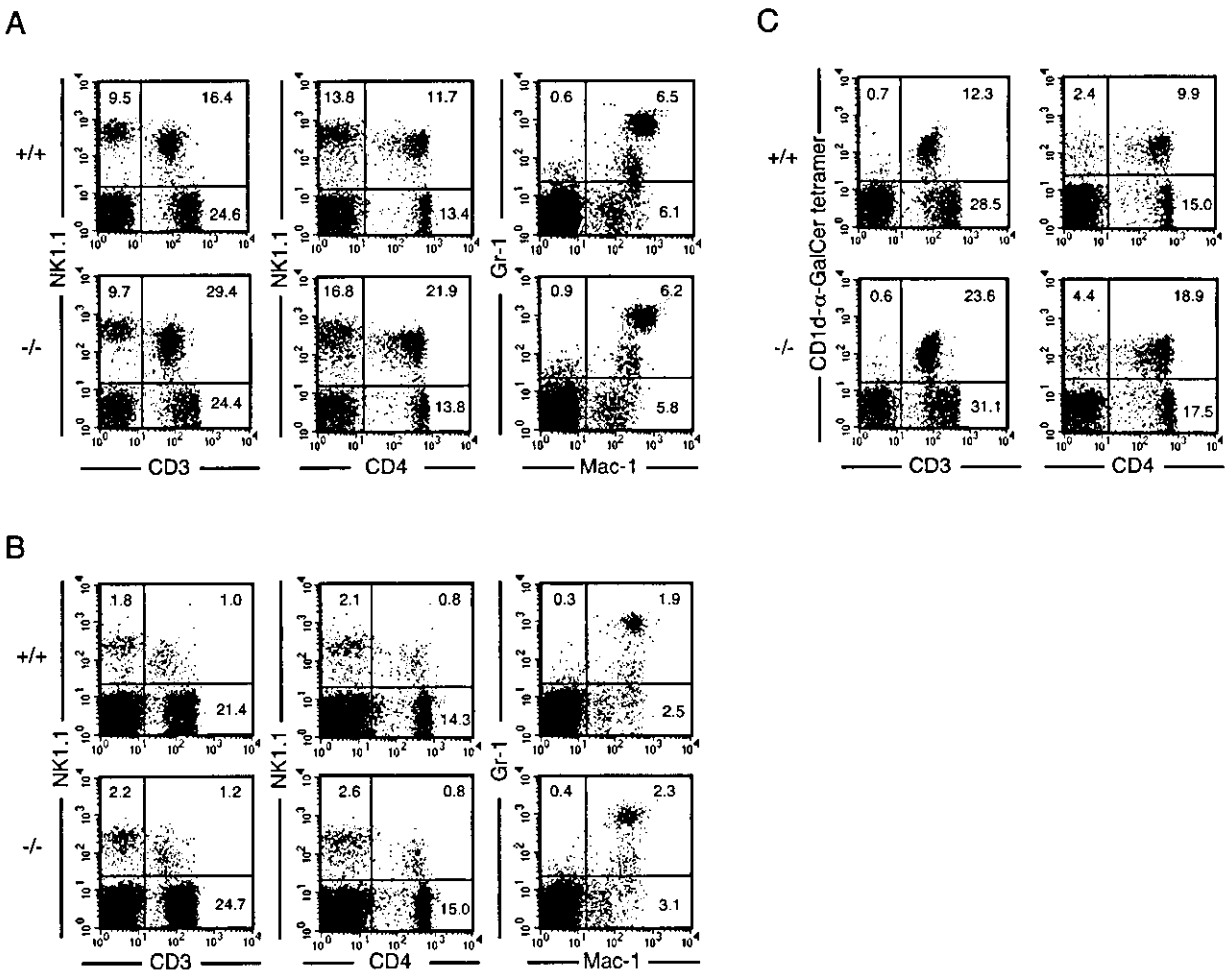

FIGURE 2. Flow cytometric analysis of mononuclear cells in LECT2$^{-/-}$ mice. Two-color staining for CD3 and NK1.1, CD4 and NK1.1, and Mac-1 and Gr-1 against MNCs from the liver (*A*) or the spleen (*B*) was performed. *C*, Hepatic MNCs were stained with CD1d-α-GalCer tetramer and anti-CD3 Ab, and CD1d-α-GalCer tetramer and anti-CD4 Ab. The numbers in the small panels indicate the representative percentages of fluorescence-positive cells in corresponding areas in six mice.

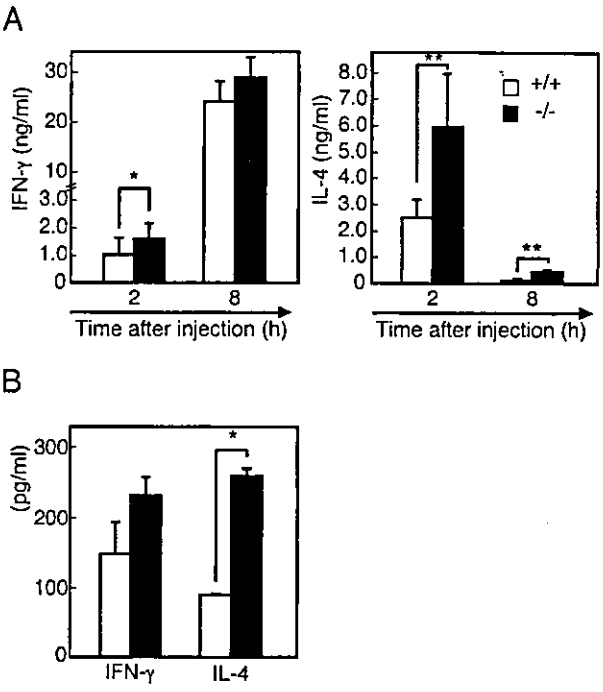

FIGURE 3. Effect of α-GalCer treatment. *A*, IFN-γ and IL-4 expression of mice administered i.p. with α-GalCer (100 μg/kg; $n = 6$ at each time point). *, $p < 0.05$; **, $p < 0.01$. The data are expressed as the mean ± SD. *B*, IFN-γ and IL-4 production by MNCs. MNCs from the liver (2×10^6 cells/ml) were cultured in RPMI 1640 supplemented with 2% FBS. Cytokines released into the culture supernatants were measured 24 h after treatment with α-GalCer (100 ng/ml). The mean values of the results obtained in triplicate are shown with the SD. The data shown are representative of four experiments.

type mice (16.0 ± 4.6% in wild-type vs 26.1 ± 6.2% in LECT2$^{-/-}$; $p < 0.01$; $n = 6$; Fig. 2*A*). The proportion of CD4$^+$ NK1.1$^+$ cells in the livers of LECT2$^{-/-}$ mice also increased compared with that in wild-type mice (11.1 ± 3.5% in wild-type vs 19.3 ± 4.8% in LECT2$^{-/-}$; $p < 0.01$; $n = 6$; Fig. 2*A*). Furthermore, the proportion of CD4$^+$ among the CD3^{int} NK1.1$^+$ cells of LECT2$^{-/-}$ mice was higher than that in wild-type mice (70.1 ± 6.9% in wild-type vs 79.4 ± 1.2% in LECT2$^{-/-}$; $p < 0.01$; $n = 6$). In contrast, there were no differences in the contents of other cell types such as CD3$^+$ NK1.1$^-$ cells (i.e., conventional T cells), CD3$^-$ NK1.1$^+$ cells (i.e., NK cells), or granulocytes (Fig. 2*A*). The total amounts of MNCs obtained from the livers of wild-type and LECT2$^{-/-}$ mice were also comparable ($2.3 \pm 0.4 \times 10^6$ cells in wild-type vs $2.2 \pm 0.7 \times 10^6$ cells in LECT2$^{-/-}$; $n = 6$; Fig. 2*A*). We also examined the proportions of immune cells in spleen, thymus, and bone marrow, but could find no significant differences (Fig. 2*B*; data not shown). These results suggest that LECT2$^{-/-}$ mice contain an increase in the proportion of hepatic NKT cells. The majority of NKT cells express invariant Vα14-Jα18 for TCR that bind to a glycolipid Ag α-GalCer, presented by CD1d. Invariant Vα14 NKT cells can be detected by using CD1d tetramer loaded with α-GalCer (21, 23, 24). LECT2$^{-/-}$ mice contained approximately twice the proportion of CD3^{int} CD1d-α-GalCer tetramer$^+$ (12.2 ± 3.5% in wild-type vs 21.7 ± 3.6% in LECT2$^{-/-}$; $p < 0.01$; $n = 6$) and CD4$^+$ CD1d-α-GalCer tetramer$^+$ cells (9.7 ± 3.0% in wild-type vs 17.7 ± 3.0% in LECT2$^{-/-}$; $p < 0.01$; $n = 6$) in the liver (Fig. 2*C*). We also confirmed by semiquantitative RT-PCR analysis that the expression of Vα14-Jα18 transcripts was definitely high in the livers of LECT2$^{-/-}$ mice (data not shown).

Responsiveness to α-GalCer treatment

NKT cells express high levels of cytokines, especially IFN-γ and IL-4, in specific response to α-GalCer treatment both in vivo and in vitro (25). As previously stated, LECT2$^{-/-}$ mice contain approximately twice the proportion of Vα14 NKT cells that are found in wild-type mice. To address the specific reactivity of NKT cells, we next measured cytokine production after the i.p. administration of α-GalCer to LECT2$^{-/-}$ mice and wild-type mice. Two hours after this treatment, LECT2$^{-/-}$ mice produced a significantly higher level of IL-4 and a slightly increased IFN-γ level compared with wild-type mice (Fig. 3*A*). We also measured the release of IFN-γ and IL-4 from cultured hepatic MNCs after stimulation with α-GalCer. As Fig. 3*B* indicates, higher amounts of IFN-γ and IL-4 were produced from the MNCs of LECT2$^{-/-}$ mice.

Cytotoxicity assay

We next examined two types of cytotoxicity of MNCs prepared from the liver and spleen of wild-type and LECT2$^{-/-}$ mice. NK cell-sensitive cytotoxicity primarily mediated by the perforin-granzyme system was assayed against YAC-1 cells, whereas NKT cell-sensitive cytotoxicity, primarily mediated by the Fas/FasL system, was assayed against syngeneic thymocytes (13, 22, 26–28). Hepatic MNCs from LECT2$^{-/-}$ mice showed substantially greater cytotoxicity against syngeneic thymocytes than did those from wild-type mice (Fig. 4), indicating that the Fas/FasL-mediated cytotoxicity of hepatic MNCs in LECT2$^{-/-}$ mice was much higher than that in wild-type mice. We also observed a slight increase in cytotoxicity in hepatic MNCs from LECT2$^{-/-}$ mice against YAC-1 cells (Fig. 4). The cytotoxicity of splenocytes against syngeneic thymocytes and YAC-1 cells was comparable between wild-type and LECT2$^{-/-}$ mice (Fig. 4).

Con A-induced hepatitis

Growing evidence indicates that NKT cells contribute significantly to the onset of Con A-induced hepatitis by expression of IL-4 and activation of cytotoxic systems (14–16). To examine whether the increase in NKT cells in LECT2$^{-/-}$ mice affects susceptibility to Con A-induced hepatitis, LECT2$^{-/-}$ and wild-type mice were injected i.v. with Con A. Serum GPT activity in LECT2$^{-/-}$ mice was elevated within 5 h after Con A administration compared with that in wild-type mice (Fig. 5*A*). In LECT2$^{-/-}$ mice only, histological examination showed a focal degenerative change, and cell clusters consisting of apoptotic cells could be detected in the liver 5 h after Con A injection (Fig. 5*B*). Con A-induced hepatitis requires the activation of immune cells accompanied by the secretion of various cytokines (13–16, 29). We therefore measured serum

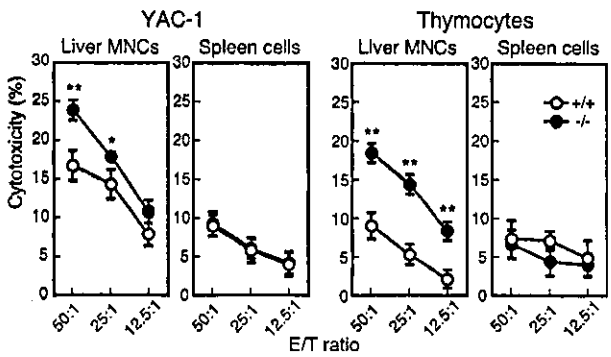

FIGURE 4. Cytotoxicity assays. MNCs were prepared from the liver and spleen of wild-type and LECT2$^{-/-}$ mice. NKT cell-sensitive cytotoxicity was determined using syngeneic B6 thymocytes as target cells. NK cell-sensitive cytotoxicity was determined using YAC-1 cells. Triplicate cultures lasted 4 h at the indicated E:T cell ratio. *, $p < 0.05$; **, $p < 0.01$.

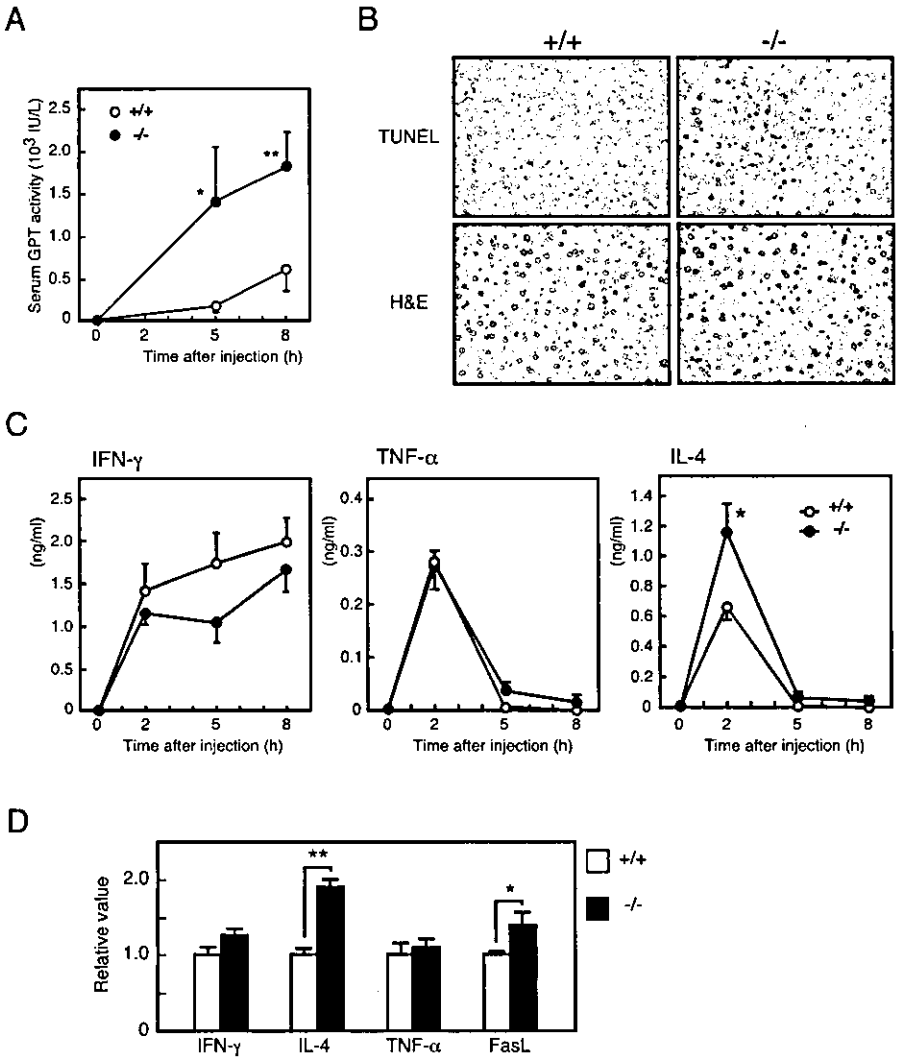

FIGURE 5. Con A-induced hepatitis. *A*, Serum GPT levels (mean ± SD) of wild-type (○) and LECT2$^{-/-}$ (●) mice were measured as described in *Materials and Methods* (n = 8 at each time point). *, $p < 0.05$; **, $p < 0.01$. *B*, Mice treated with Con A were killed at 5 h, and livers were processed for histological analysis. In situ TUNEL staining of liver sections was performed to identify apoptotic cells. *C*, Changes of serum IFN-γ, TNF-α, and IL-4 levels (mean ± SD) in Con A-induced hepatitis. The serum concentrations of cytokines from wild-type (○) and LECT2$^{-/-}$ (●) mice were measured as described above (n = 8 at each time point). *, $p < 0.05$. *D*, Quantitative real-time RT-PCR analysis for cytokine expression. Total liver RNAs were prepared from mice 2 h after Con A injection. The relative ratios of PCR products detected in wild-type mice (assigned a value of 1) vs LECT2$^{-/-}$ mice are indicated (n = 5). *, $p < 0.05$; **, $p < 0.01$.

cytokine levels during the course of the liver injury. Significant elevation of IL-4 in the serum was observed in LECT2$^{-/-}$ mice (Fig. 5*C*). In contrast, the levels of TNF-α and IFN-γ were not significantly different between wild-type and LECT2$^{-/-}$ mice (Fig. 5*C*). Furthermore, the levels of IL-6 and IL-10 in these mouse types were also comparable (data not shown). To compare the local expression of cytokines, quantitative real-time RT-PCR analysis of liver tissue RNA at 2 h after Con A injection was performed. The results revealed that IL-4 and FasL expression in the liver of LECT2$^{-/-}$ mice was significantly higher than that in wild-type liver (Fig. 5*D*). FasL is known as an effector molecule in Con A-induced hepatic injury, and NKT cells primarily express it (16). Thus, the increased hepatic LECT2$^{-/-}$ NKT cells contribute to the severity of Con A-induced hepatitis.

FasL expression and increase in annexin V-positive CD3^{int} NK1.1^{+} cells during Con A-induced hepatitis

To examine whether the NKT cells of LECT2$^{-/-}$ mice indeed expressed large amounts of FasL upon stimulation with Con A, the proportion of CD3^{int} NK1.1^{+} cells expressing FasL was determined by flow cytometric analysis. Three hours after Con A injection, the CD3^{int} NK1.1^{+} cells in LECT2$^{-/-}$ mice expressed approximately twice the amount of FasL that was found in wild-type mice (Fig. 6*A*). Conventional T cells of both wild-type and LECT2$^{-/-}$ mice expressed scarcely any FasL (Fig. 6*A*).

Next, we analyzed the proportion of NKT cells that become apoptotic upon stimulation with Con A, because current evidence suggests that hepatic NKT cells are eliminated by apoptosis after Con A injection (16). The three-color staining of CD3^{int} NK1.1^{+} and annexin-V demonstrated that hepatic CD3^{int} NK1.1^{+} cells of both wild-type and LECT2$^{-/-}$ mice decreased 3 h after Con A injection, and the proportion of annexin V-positive cells was higher in LECT2$^{-/-}$ mice. In contrast, conventional T cells were not stained with annexin V (Fig. 6*B*). These results suggest that hepatic NKT cells in LECT2$^{-/-}$ mice showed increased activation-dependent apoptosis, as is the case in wild-type mice.

Discussion

LECT2 was originally noted for its possible neutrophil chemotactic activity (1). In addition, it was independently reported to be a growth-stimulating factor for chondrocytes and osteoblasts and was named chondromodulin II (6). To determine the function of LECT2 in vivo, we generated LECT2$^{-/-}$ mice. In some preliminary experiments we could not easily find any clear differences related to the above two activities. Therefore, based on the possible roles of LECT2 in liver injury and its tissue-specific expression (2, 3), we focused on the liver.

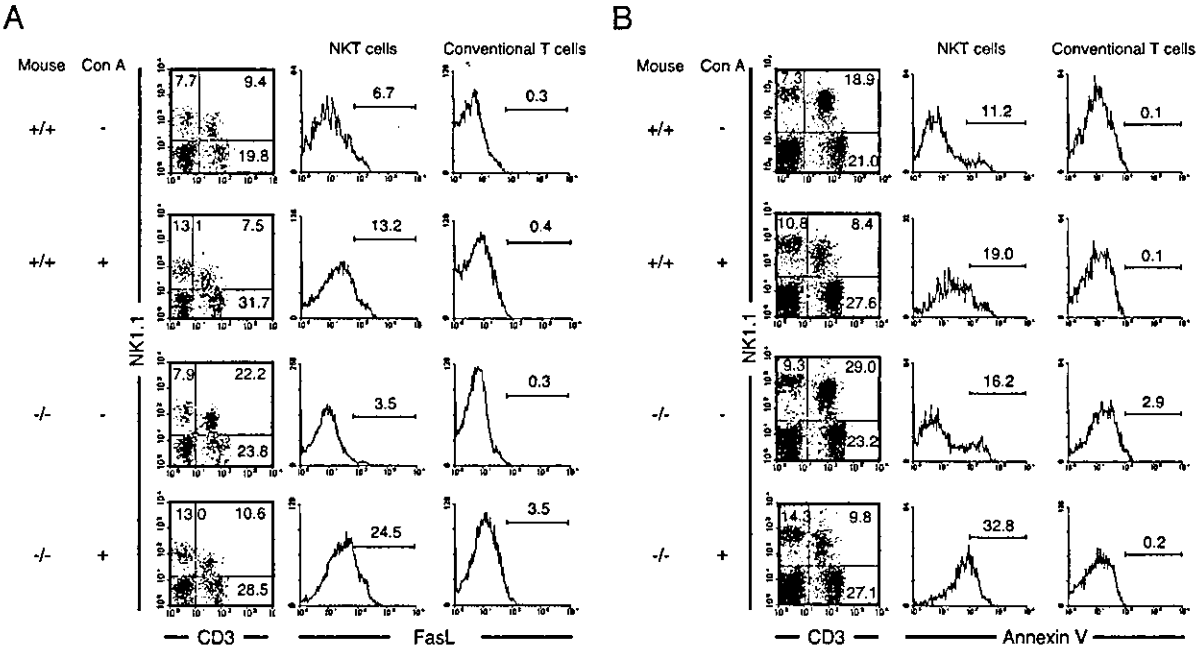

FIGURE 6. Detections of NKT cells expressing FasL or annexin V-positive NKT cells during Con A-induced hepatitis. *A*, NKT cells or conventional T cells that express FasL were detected by three-color staining for CD3, NK1.1, and FasL. Hepatic MNCs were prepared 3 h after injection with Con A or control saline. *B*, Increase in annexin V-positive NKT cells in the livers of mice challenged with Con A. Hepatic MNCs were isolated 3 h after the Con A challenge. Three-color staining was performed for CD3, NK1.1, and annexin V.

In the present study we found an increased proportion of hepatic CD3^{int} NK1.1$^+$ and CD4$^+$ NK1.1$^+$ cells in LECT2$^{-/-}$ mice compared with that in wild-type mice (Fig. 2*A*). Moreover, we observed that the proportion of hepatic CD3^{int} CD1d-α-GalCer tetramer$^+$ cells in LECT2$^{-/-}$ mice was about double that in wild-type mice (Fig. 2*C*), indicating that LECT2$^{-/-}$ mice have an increased proportion of hepatic Vα14 NKT cells. The production of IL-4 and IFN-γ 2 h after administration of α-GalCer in mice would be primarily derived from NKT cells (30). Furthermore, the higher production of both cytokines from the hepatic MNCs treated with α-GalCer is consistent with this result. Therefore, the differences in the levels of IL-4 and IFN-γ after stimulation with α-GalCer in vivo and in vitro could be explained by the increased number of NKT cells in LECT2$^{-/-}$ mice. In addition, the Fas/FasL-sensitive cytotoxicity of hepatic MNCs in LECT2$^{-/-}$ mice was much higher than that in wild-type mice. In contrast, this cytotoxicity of spleen cells from both wild-type and LECT2$^{-/-}$ mice was comparable. We also could find no significant differences in the percentage of CD3^{int} NK1.1$^+$ cells in the spleen cells of LECT2$^{-/-}$ and wild-type mice. Therefore, augmentation of the Fas/FasL-sensitive cytotoxicity shown in hepatic MNCs was possibly due to the increased percentage of NKT cells in LECT2$^{-/-}$ mice. In addition, the NK-sensitive cytotoxicity in hepatic MNCs from LECT2$^{-/-}$ mice was slightly higher than that in MNCs from wild-type mice. At present, although the reason for this slight enhancement is not clear, the cytotoxicity of hepatic NK cells also might be enhanced in LECT2$^{-/-}$ mice. Thus, all these results indicate that LECT2$^{-/-}$ mice show an increase in hepatic NKT cells, which appear to function as they do in wild-type mice.

To explore the biological effects of the increased number of hepatic NKT cells in LECT2$^{-/-}$ mice, we compared wild-type and LECT2$^{-/-}$ mice using the Con A-induced hepatitis model. The onset of Con A-induced hepatitis requires a complicated process of activation of cytokines from immune cells. Both IFN-γ and TNF-α play crucial roles in Con A-induced hepatitis (29, 31). Recent reports have pointed out that activated NKT cells expressing IL-4 also play an essential role in Con A-induced hepatitis and mediate subsequent activation of the cytotoxic pathways (14–16). We showed that LECT2$^{-/-}$ mice were clearly sensitive to Con A-induced hepatitis (Fig. 5, *A* and *B*), and that the levels of IL-4 and FasL in LECT2$^{-/-}$ mice were higher than those in wild-type mice (Fig. 5, *C* and *D*). These findings strongly suggest that a higher level of IL-4 expression induces excessive FasL and also probably granzyme B (15), resulting in the production of a number of apoptotic hepatocytes (Fig. 5*B*) and a larger proportion of annexin V-positive hepatic CD3^{int} NK1.1$^+$ cells (Fig. 6). Recently, several reports showed that the NK1.1 marker of CD3^{int} NK1.1$^+$ cells is down-modulated on activation (32–35). Therefore, the decrease in CD3^{int} NK1.1$^+$ cells after Con A challenge in both wild-type and LECT2$^{-/-}$ mice (Fig. 6) might be due not only to apoptosis of NKT cells, but also to down-regulation of the NK1.1 marker.

The reason for the increase in hepatic NKT cells in LECT2$^{-/-}$ mice is an important issue. LECT2 might participate in the differentiation, development, or both of NKT cell lineages. There is considerable evidence for genes that positively regulate the development of NK or NKT lineages (36). In contrast, LECT2$^{-/-}$ mice have an increase in NKT cells in the liver, suggesting that LECT2 might negatively regulate the development of NKT cell lineages. However, considering that there were no obvious differences in CD3^{int} NK1.1$^+$ cells of spleen, thymus, and bone marrow (Fig. 2*C*; data not shown), a role for LECT2 might be related to the homeostasis of NKT cells in the liver. For example, LECT2 might control an immune state in the liver by regulating the selection and/or expansion of hepatic NKT cells or the homing activity of NKT cells toward the liver. Moreover, a distinctive feature of NKT cells in LECT2$^{-/-}$ mice is that the difference in IL-4 production between wild-type and LECT2$^{-/-}$ mice is greater than that in IFN-γ production upon stimulation with α-GalCer. The possible IL-4 dominance might be related to the observation that mice containing an increased number of NKT cells tend to be IL-4 dominant (37–40), or immature NKT cell lineages tend to exhibit the

Th2-type-dominant phenotype (41, 42). It is possible that an imbalance in the proportion of NKT cells in LECT2$^{-/-}$ mice affects an immune state, which is associated with the pathogenesis of certain immune diseases.

In summary, our results revealed that the number of hepatic NKT cells was increased in LECT2$^{-/-}$ mice and suggested that LECT2 may play an important role in the homeostasis of NKT cells in the liver. Although a deficiency of LECT2 does not cause any significant abnormality in mice under physiological conditions, they become susceptible to Con A-induced hepatitis, probably due to excessive production of IL-4 and FasL from NKT cells. Thus, it is possible that LECT2 might be involved in the pathogenesis of hepatitis or other inflammatory diseases in humans through modulation of NKT cell activity.

Acknowledgments

We kindly thank Dr. Yasuhiko Koezuka (Kirin Brewery, Pharmaceutical Research Laboratory) for useful comments.

References

1. Yamagoe, S., Y. Yamakawa, Y. Matsuo, J. Minowada, S. Mizuno, and K. Suzuki. 1996. Purification and primary amino acid sequence of a novel neutrophil chemotactic factor LECT2. *Immunol. Lett. 52:9.*
2. Yamagoe, S., S. Mizuno, and K. Suzuki. 1998. Molecular cloning of human and bovine LECT2 having a neutrophil chemotactic activity and its specific expression in the liver. *Biochim. Biophys. Acta 1396:105.*
3. Segawa, Y., Y. Itokazu, N. Inoue, T. Saito, and K. Suzuki. 2001. Possible changes in expression of chemotaxin LECT2 mRNA in mouse liver after concanavalin A-induced hepatic injury. *Biol. Pharm. Bull. 24:425.*
4. Ness, S. A., Å. Marknell, and T. Graf. 1989. The v-*myb* oncogene product binds to and activates the promyelocyte-specific *mim-1* gene. *Cell 59:1115.*
5. Fujiki, K., D.-H. Shin, M. Nakao, and T. Yano. 2000. Molecular cloning of carp (*Cyprinus carpio*) leucocyte cell-derived chemotaxin 2, glia maturation factor β, CD45 and lysozyme C by use of suppression subtractive hybridization. *Fish Shellfish Immunol. 10:643.*
6. Hiraki, Y., H. Inoue, J. Kondo, A. Kamizono, Y. Yoshitake, C. Shukunami, and F. Suzuki. 1996. A novel growth-promoting factor derived from fetal bovine cartilage, chondromodulin. II. Purification and amino acid sequence. *J. Biol. Chem. 271:22657.*
7. Kameoka, Y., S. Yamagoe, Y. Hatano, T. Kasama, and K. Suzuki. 2000. Val^{58}Ile polymorphism of the neutrophil chemoattractant *LECT2* and rheumatoid arthritis in the Japanese population. *Arthritis Rheum. 43:1419.*
8. Tiegs, G., J. Hentschel, and A. Wendel. 1992. A T cell-dependent experimental liver injury in mice inducible by concanavalin A. *J. Clin. Invest. 90:196.*
9. Bendelac, A. 1995. Mouse NK$^+$ T cells. *Curr. Opin. Immunol. 7:367.*
10. Bendelac, A., M. N. Rivera, S.-H. Park, and J. H. Roark. 1997. Mouse CD1-specific NK1 T cells: development, specificity, and function. *Annu. Rev. Immunol. 15:535.*
11. MacDonald, H. R. 1995. NK1.1$^+$ T cell receptor-α/β$^+$ cells: new clues to their origin, specificity, and function. *J. Exp. Med. 182:633.*
12. Godfrey, D. I., K. J. Hammond, L. D. Poulton, M. J. Smyth, and A. G. Baxter. 2000. NKT cells: facts, functions and fallacies. *Immunol. Today 21:573.*
13. Abo, T., T. Kawamura, and H. Watanabe. 2000. Physiological responses of extrathymic T cells in the liver. *Immunol. Rev. 174:135.*
14. Toyabe, S., S. Seki, T. Iiai, K. Takeda, K. Shirai, H. Watanabe, H. Hiraide, M. Uchiyama, and T. Abo. 1997. Requirement of IL-4 and liver NK1$^+$ T cells for concanavalin A-induced hepatic injury in mice. *J. Immunol. 159:1537.*
15. Kaneko, Y., M. Harada, T. Kawano, M. Yamashita, Y. Shibata, F. Gejyo, T. Nakayama, and M. Taniguchi. 2000. Augmentation of Vα14 NKT cell-mediated cytotoxicity by interleukin 4 in an autocrine mechanism resulting in the development of concanavalin A-induced hepatitis. *J. Exp. Med. 191:105.*
16. Takeda, K., Y. Hayakawa, L. van Kaer, H. Matsuda, H. Yagita, and K. Okumura. 2000. Critical contribution of liver natural killer T cells to a murine model of hepatitis. *Proc. Natl. Acad. Sci. USA 97:5498.*
17. Yamagoe, S., T. Watanabe, S. Mizuno, and K. Suzuki. 1998. The mouse *Lect2* gene: cloning of cDNA and genomic DNA, structural characterization and chromosomal localization. *Gene 216:171.*
18. Soriano, P., C. Montgomery, R. Geske, and A. Bradley. 1991. Targeted disruption of the c-*src* proto-oncogene leads to osteopetrosis in mice. *Cell 64:693.*
19. Horai, R., M. Asano, K. Sudo, H. Kanuka, M. Suzuki, M. Nishihara, M. Takahashi, and Y. Iwakura. 1998. Production of mice deficient in genes for interleukin (IL)-1α, IL-1β, IL-1α/β, and IL-1 receptor antagonist shows that IL-1β is crucial in turpentine-induced fever development and glucocorticoid secretion. *J. Exp. Med. 187:1463.*
20. Watanabe, H., K. Ohtsuka, M. Kimura, Y. Ikarashi, K. Ohmori, A. Kusumi, T. Ohteki, S. Seki, and T. Abo. 1992. Details of an isolation method for hepatic lymphocytes in mice. *J. Immunol. Methods 146:145.*
21. Stanic, A. K., A. D. De Silva, J.-J. Park, V. Sriram, S. Ichikawa, Y. Hirabayashi, K. Hayakawa, L. van Kaer, R. R. Brutkiewicz, and S. Joyce. 2003. Defective presentation of the CD1d1-restricted natural Va14Ja18 NKT lymphocyte antigen caused by β-D-glucosylceramide synthase deficiency. *Proc. Natl. Acad. Sci. USA 100:1849.*
22. Moroda, T., T. Iiai, S. Suzuki, A. Tsukahara, T. Tada, M. Nose, K. Hatakeyama, S. Seki, K. Takeda, H. Watanabe, et al. 1997. Autologous killing by a population of intermediate T-cell receptor cells and its NK1.1$^+$ and NK1.1$^-$ subsets, using Fas ligand/Fas molecules. *Immunology 91:219.*
23. Benlagha, K., A. Weiss, A. Beavis, L. Teyton, and A. Bendelac. 2000. In vivo identification of glycolipid antigen-specific T cells using fluorescent CD1d tetramers. *J. Exp. Med. 191:1895.*
24. Matsuda, J. L., O. V. Naidenko, L. Gapin, T. Nakayama, M. Taniguchi, C.-R. Wang, Y. Koezuka, and M. Kronenberg. 2000. Tracking the response of natural killer T cells to a glycolipid antigen using CD1d tetramers. *J. Exp. Med. 192:741.*
25. Kawano, T., J. Cui, Y. Koezuka, I. Toura, Y. Kaneko, K. Motoki, H. Ueno, R. Nakagawa, H. Sato, E. Kondo, et al. 1997. CD1d-restricted and TCR-mediated activation of Vα14 NKT cells by glycosylceramides. *Science 278:1626.*
26. Osman, Y., T. Kawamura, T. Naito, K. Takeda, L. van Kaer, K. Okumura, and T. Abo. 2000. Activation of hepatic NKT cells and subsequent liver injury following administration of α-galactosylceramide. *Eur. J. Immunol. 30:1919.*
27. Miyaji, C., H. Watanabe, R. Miyakawa, H. Yokoyama, C. Tsukada, Y. Ishimoto, S. Miyazawa, and T. Abo. 2002. Identification of effector cells for TNFα-mediated cytotoxicity against WEHI164S cells. *Cell. Immunol. 216:43.*
28. Hayakawa, Y., K. Takeda, H. Yagita, S. Kakuta, Y. Iwakura, L. van Kaer, I. Saiki, and K. Okumura. 2001. Critical contribution of IFN-γ and NK cells, but not perforin-mediated cytotoxicity, to anti-metastatic effect of α-galactosylceramide. *Eur. J. Immunol. 31:1720.*
29. Mizuhara, H., E. O'Neill, N. Seki, T. Ogawa, C. Kusunoki, K. Otsuka, S. Satoh, M. Niwa, H. Senoh, and H. Fujiwara. 1994. T cell activation-associated hepatic injury: mediation by tumor necrosis factors and protection by interleukin 6. *J. Exp. Med. 179:1529.*
30. Carnaud, C., D. Lee, O. Donnars, S.-H. Park, A. Beavis, Y. Koezuka, and A. Bendelac. 1999. Cross-talk between cells of the innate immune system: NKT cells rapidly activate NK cells. *J. Immunol. 163:4647.*
31. Gantner, F., M. Leist, A. W. Lohse, P. G. Germann, and G. Tiegs. 1995. Concanavalin A-induced T-cell-mediated hepatic injury in mice: the role of tumor necrosis factor. *Hepatology 21:190.*
32. Chen, H., H. Huang, and W. E. Paul. 1997. NK1.1$^+$ CD4$^+$ T cells lose NK1.1 expression upon in vitro activation. *J. Immunol. 158:5112.*
33. Wilson, M. T., C. Johansson, D. Olivares-Villagómez, A. K. Singh, A. K. Stanic, C.-R. Wang, S. Joyce, M. J. Wick, and L. van Kaer. 2003. The response of natural killer T cells to glycolipid antigens is characterized by surface receptor down-modulation and expansion. *Proc. Natl. Acad. Sci. USA 100:10913.*
34. Crowe, N. Y., A. P. Uldrich, K. Kyparissoudis, K. J. L. Hammond, Y. Hayakawa, S. Sidobre, R. Keating, M. Kronenberg, M. J. Smyth, and D. I. Godfrey. 2003. Glycolipid antigen drives rapid expansion and sustained cytokine production by NK T cells. *J. Immunol. 171:4020.*
35. Emoto, M., and S. H. E. Kaufmann. 2003. Liver NKT cells: an account of heterogeneity. *Trends Immunol. 24:364.*
36. Kronenberg, M., and L. Gapin. 2002. The unconventional lifestyle of NKT cells. *Nat. Rev. Immunol. 2:557.*
37. Laloux, V., L. Beaudoin, D. Jeske, C. Carnaud, and A. Lehuen. 2001. NK T cell-induced protection against diabetes in Vα14-Jα281 transgenic nonobese diabetic mice is associated with a Th2 shift circumscribed regionally to the islets and functionally to islet autoantigen. *J. Immunol. 166:3749.*
38. Gunperz, J. E., S. Miyake, T. Yamamura, and M. B. Brenner. 2002. Functionally distinct subsets of CD1d-restricted natural killer T cells revealed by CD1d tetramer staining. *J. Exp. Med. 195:625.*
39. Lee, P. T., K. Benlagha, L. Teyton, and A. Bendelac. 2002. Distinct functional lineages of human Vα24 natural killer T cells. *J. Exp. Med. 195:637.*
40. Chen, H., and W. E. Paul. 1997. Cultured NK1.1$^+$ CD4$^+$ T cells produce large amounts of IL-4 and IFN-γ upon activation by anti-CD3 or CD1. *J. Immunol. 159:2240.*
41. Pellicci, D. G., K. J. L. Hammond, A. P. Uldrich, A. G. Baxter, M. J. Smyth, and D. I. Godfrey. 2002. A natural killer T (NKT) cell developmental pathway involving a thymus-dependent NK1.1$^-$ CD4$^+$ CD1d-dependent precursor stage. *J. Exp. Med. 195:835.*
42. Benlagha, K., T. Kyin, A. Beavis, L. Teyton, and A. Bendelac. 2002. A thymic precursor to the NK T cell lineage. *Science 296:553.*

Critical roles of interferon regulatory factor 4 in CD11b^{high}CD8α^- dendritic cell development

Shoichi Suzuki*, Kiri Honma†, Toshifumi Matsuyama‡§, Kazuo Suzuki¶, Kan Toriyama‖, Ichinose Akitoyo**, Kazuo Yamamoto‡, Takashi Suematsu††, Michio Nakamura*, Katsuyuki Yui†, and Atsushi Kumatori*

Departments of *Host-Defense Biochemistry and ‖Pathology, **Central Laboratory, Institute of Tropical Medicine, †Division of Immunology, Department of Translational Medical Sciences, ‡Department of Molecular Microbiology and Immunology, and ††Electron Microscope Center, Graduate School of Biomedical Sciences, Nagasaki University, 1-12-4 Sakamoto, Nagasaki 852-8523, Japan; and ¶Laboratory of Biodefense, National Institute of Infectious Diseases, 1-23-1 Toyama, Shinjuku-ku, Tokyo 162-8640, Japan

Edited by Ralph M. Steinman, The Rockefeller University, New York, NY, and approved April 27, 2004 (received for review March 29, 2004)

IFN regulatory factors (IRFs) are a family of transcription factors that play an essential role in the homeostasis and function of immune systems. Recent studies indicated that IRF-8 is critical for the development of CD11b^{low}CD8α^+ conventional dendritic cells (DCs) and plasmacytoid DCs. Here we show that IRF-4 is important for CD11b^{high}CD8α^- conventional DCs. The development of CD11b^{high} DCs from bone marrow of IRF-4$^{-/-}$ mice was severely impaired in two culture systems supplemented with either GM-CSF or Flt3-ligand. In the IRF-4$^{-/-}$ spleen, the number of CD4$^+$CD8α^- DCs, a major subset of CD11b^{high} DCs, was severely reduced. IRF-4 and IRF-8 were expressed in the majority of CD11b^{high}CD4$^+$CD8α^- DCs and CD11b^{low}CD8α^+ DCs, respectively, in a mutually exclusive manner. These results imply that IRF-4 and IRF-8 selectively play critical roles in the development of the DC subsets that express them.

Dendritic cells (DCs) are professional antigen-presenting cells that link the innate and adaptive immune systems. They express CD11c and are composed of heterogeneous cell populations with different functions (1). At present, murine DCs have been divided into two major groups, B220$^-$ conventional DCs and B220$^+$ plasmacytoid DCs (2–5). In lymphoid organs, the conventional DCs can be divided into two subsets, CD11b^{high}CD8α^- and CD11b^{low}CD8α^+ DCs, based on the expression of surface markers (1). In the spleen, the CD11b^{high}CD8α^- subset can be further divided into CD4$^+$ and CD4$^-$ DCs (6, 7). *In vitro*, CD11b^{high}CD8α^- DCs can be generated in two bone marrow (BM) culture systems, supplemented with either granulocyte–macrophage colony-stimulating factor (GM-CSF) or Flt3 ligand (Flt3L) (8–10). CD11b^{low}CD8α^+ DCs can also be generated from a BM culture supplemented with Flt3L, although further stimulation by lipopolysaccharide (LPS) is needed to induce the expression of CD8α (10). The molecular phenomena that regulate the differentiation of these distinct subsets of DCs are poorly understood.

Transcription factors of the IFN-regulatory factor (IRF) family participate in the early host response to pathogens, immunomodulation, and hematopoietic differentiation (11). A member of the family, IRF-4, was cloned independently as a homologous member of the IRF gene family (12) and as an interacting partner of PU.1 (Pip) (13). PU.1 is an Ets family member involved in B lymphocyte and myeloid lineage development (14, 15) and is essential for the development of CD8α^- DCs (16, 17). Upon their association, IRF-4 and PU.1 undergo conformational changes, followed by binding to the DNA-binding element (18). IRF-4 is expressed at all stages of B cell development, in mature T cells (12), adult T cell leukemia cell lines (19, 20), and in macrophages (21, 22). The analysis of mice lacking IRF-4 (IRF-4$^{-/-}$) revealed that IRF-4 is essential for the function and homeostasis of both mature B and T lymphocytes (23, 24). IRF-8 (originally named IFN consensus sequence binding protein, ICSBP) is another member of the IRF family, and its structure is closely related to that of IRF-4. It can interact with PU.1 and binds to a DNA sequence similar to that bound by IRF-4 (22). Recent studies indicated that IRF-8 is critical for the development of CD11b^{low}CD8α^+ conventional DCs and plasmacytoid DCs (25–28). Here, we show that bone marrow cells from IRF-4 knockout mice have intrinsic defects in the development of CD11b^{high} DCs in two culture systems supplemented with either GM-CSF or Flt3-ligand. Mice lacking the IRF-4 gene have selective defects in splenic CD11b^{high}CD8α^- conventional DCs. IRF-4 is expressed in this subset of DCs, indicating that IRF-4 plays a critical role in the development of the DC subset that expresses it.

Methods

Mice. C57BL/6J mice were purchased from CLEA Japan (Osaka). IRF-4-deficient mice (23) and OT-II transgenic mice (29), expressing the T cell receptor specific for OVA323–339 and I-A^b, were maintained at the Laboratory Animal Center for Biomedical Research, Nagasaki University School of Medicine.

BM Cultures. The GM-CSF-supplemented BM culture was performed as described (9). The culture supernatant from a Chinese hamster ovary cell line transfected with the murine GM-CSF gene was used as the source of GM-CSF. At day 10, the nonadherent cells were harvested by gentle pipeting and were stimulated with 1 μg/ml LPS (*Escherichia coli* 0127:B8, Sigma) for 48 h. The Flt3L-supplemented BM culture was performed as described (10), except mouse Flt3L (Genzyme/Techne) was used. At day 9, the nonadherent cells were harvested by gentle pipeting and were stimulated with 1 μg/ml LPS for 24 h. For the experiments using the six-well transwell plates (Corning, NY), 5.2×10^5 BM cells (low cell density) in the lower chamber and 5×10^6 BM cells (high cell density) in the upper chamber were cultured in 4.1 ml of McCoy's medium, supplemented with 100 ng/ml Flt3L, for 10 days as described (10). For details see *Supporting Text*, which is published as supporting information on the PNAS web site.

Cell Preparation from Lymphoid Organs. Cells from thymuses and spleens were prepared as described (6). Low-density cells from spleen were also prepared as described (6).

Flow Cytometry. The cells were blocked with anti-CD16/32 antibody, rat IgG, and mouse IgG. All antibodies were purchased from BD Pharmingen, except where noted. In addition to the isotype controls, the following antibodies were used: Anti-CD16/32, FITC-conjugated anti-MHC class II (MHC-II),

This paper was submitted directly (Track II) to the PNAS office.

Abbreviations: DC, dendritic cell; BM, bone marrow; Flt3L, Flt3 ligand; GM-CSF, granulocyte–macrophage colony-stimulating factor; LPS, lipopolysaccharide; IRF, IFN-regulatory factor; PE, phycoerythrin; PerCP, peridinin chlorophyll-α protein; NPTII, neomycin phosphotransferase II; OVA, ovalbumin; MHC-II, MHC class II; NK, natural killer.

§To whom correspondence should be addressed. E-mail: tosim@net.nagasaki-u.ac.jp.

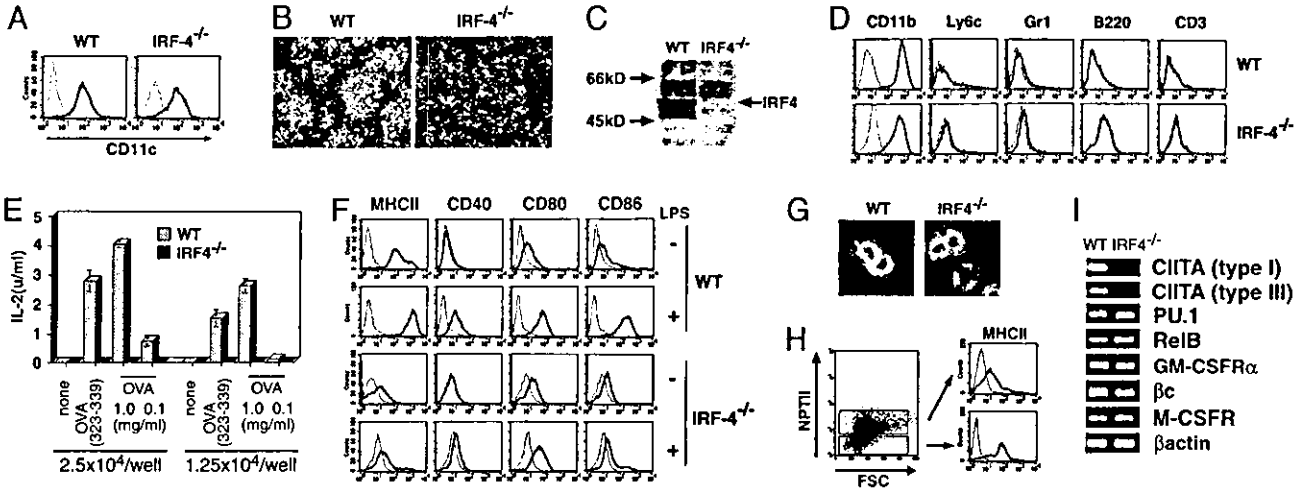

Fig. 1. Impaired DC development in the IRF-4$^{-/-}$ BM culture with GM-CSF. (*A*) The CD11c expression on nonadherent cells from GM-CSF BM cultures at day 10 was analyzed by flow cytometry. (*B*) Photographs of the cultures by phase contrast microscopy, taken at day 10. (*C*) The expression of IRF-4 in the CD11c$^+$ cells was assessed by immunoblotting. Lysates from 2.5 × 10^5 cells were subjected to electrophoresis. (*D*) The lineage marker expression on the CD11c$^+$ cells was analyzed by flow cytometry. (*E*) The antigen-presenting ability of the CD11c$^+$ cells for whole OVA and its peptide (323–339 amino acid residues) to OVA-specific CD4$^+$ T cells was examined. (*F*) MHC-II and costimulatory factor expression by the nonstimulated and LPS-stimulated CD11c$^+$ cells was examined. (*G*) The morphology of LPS-stimulated CD11c$^+$ cells was observed by phase contrast microscopy. (*H*) Wild-type and IRF-4$^{-/-}$ BM cells were cocultured. After 10 days, the expression of MHC-II on the cells was analyzed. NPTII expression by the wild-type and the IRF-4$^{-/-}$ cells was distinguished by flow cytometry with anti-MHC-II and anti-NPTII. (*I*) The expression of several transcription factor and cytokine receptor genes involved in DC development was analyzed by RT-PCR.

anti-CD8, and anti-Gr-1; phycoerythrin (PE)-conjugated anti-CD11c; CyChrome-conjugated anti-CD4; peridinin chlorophyll-α protein (PerCP)-conjugated anti-B220; biotin-conjugated anti-CD11b, anti-B220, and anti-Ly6c; PE-conjugated anti-CD40, anti-CD80, and anti-CD86 from Immunotech; biotin-conjugated anti-CD8 and anti-MHC-II, PE-conjugated anti-CD3, and allophycocyanin-conjugated anti-CD4 from eBioscience; and anti-IRF-4 and anti-IRF-8 from Santa Cruz Biotechnology. The binding of biotinylated antibodies was detected with PerCP-Cy5.5- or CyChrome-conjugated streptavidin. Analyses of stained cells were performed on a FACScan or FACSCalibur with the CELLQUEST software (BD Bioscience).

Intracellular Staining. For the analysis of neomycin phosphotransferase II (NPTII), cells were fixed and permeabilized with the Fix and Perm kit (Caltag), and were incubated with anti-NPTII (Upstate Biotechnology) followed by ant-rabbit IgG-biotin (Santa Cruz Biotechnology) and streptavidin-CyChrome. For analyses of IRF-4 and IRF-8, cells were fixed with 1% paraformaldehyde (Wako) and permeabilized with 0.5% Triton X-100 (Wako). The permeabilized cells were incubated with the anti-IRF-4 or IRF-8 antibody, followed by anti-goat IgG-Alexa Fluor 488 (Molecular Probes)

Western Blot Analysis. Cell lysates were prepared as described (30), with modifications (see supporting information). Immunoblotting was performed as described (31).

RT-PCR. Total RNA was prepared from cells as described (31). The cDNA synthesized from the total RNA by using ReverTra Ace (Toyobo) was subjected to PCR amplification using EX *Taq* (Takara) and the following primers: CIITA (sense), type I exon1: GACTTTCTTGAGCTGGGTCTG; type III exon1: CTGGCCCTTCTGGGTCTTAC; CIITA (antisense), common exon2: TCTTCATCCAGTTCCATGTCC. All of the other primer sequences are available on request.

Antigen-Presentation Assay. The ability of DCs to activate antigen-specific T cells was monitored by the secretion of IL-2 from CD4$^+$ T cells of OT-II mice. Purified CD4$^+$ T cells from OT-II mice (4 × 10^5 per well) were stimulated with ovalbumin (OVA) or its peptide and various numbers of DCs. After 48 h, the IL-2 level in the culture supernatant was determined by a sandwich ELISA with a biotin-conjugated anti-IL-2 antibody (BD Pharmingen) and avidin-alkaline phosphatase (Jackson ImmunoResearch).

Results

Defective DC Development in IRF-4$^{-/-}$ BM Culture. During analyses of the DC-specific regulatory mechanisms of the gp91^{phox} gene, which is expressed in a cell type-specific manner (32–34), we found that the IRF-4 protein was expressed in human DCs and bound to the Ets/IRF composite element of the promoter together with PU.1 (data not shown). This observation was consistent with the recent studies on DC-associated factors, which revealed the expression of IRF-4 mRNA in human DCs (35, 36). Therefore, we used the GM-CSF-supplemented cultures of BM from IRF-4$^{-/-}$ mice to determine the role of IRF-4 in DC development and function. Nonadherent CD11c$^+$ cells were generated from BM cells of IRF-4$^{-/-}$ mice as well as wild-type mice (Fig. 1*A*). Surprisingly, CD11c$^+$ cells from IRF-4$^{-/-}$ BM failed to form DC clusters (Fig. 1*B*) and showed no veil processes (Fig. 5, which is published as supporting information on the PNAS web site). A Western blot analysis demonstrated that CD11c$^+$ cells from wild-type mice expressed the IRF-4 protein, but those from IRF-4$^{-/-}$ mice did not (Fig. 1*C*). Flow cytometry analysis showed that CD11c$^+$ cells from both wild-type and IRF-4$^{-/-}$ BM expressed CD11b at high levels but did not express B220, CD3, Gr-1, and Ly6c (Fig. 1*D*).

Next, we evaluated their ability to present the OVA protein (1 and 0.1 mg/ml) or its peptide (323–339 amino acid residues) to OVA-specific CD4$^+$ T cells from OT-II mice (29). The wild-type DCs stimulated IL-2 production of the T cells in antigen dose- and DC number-dependent manners. However, CD11c$^+$ cells from IRF-4$^{-/-}$ BM were unable to stimulate IL-2 production by OVA-specific T cells (Fig. 1*E*). We also analyzed their expression of the surface antigens associated with antigen presentation (Fig. 1*F*). The expression of MHC-II on CD11c$^+$ cells from IRF-4$^{-/-}$ BM was extremely low, consistent with their defects in

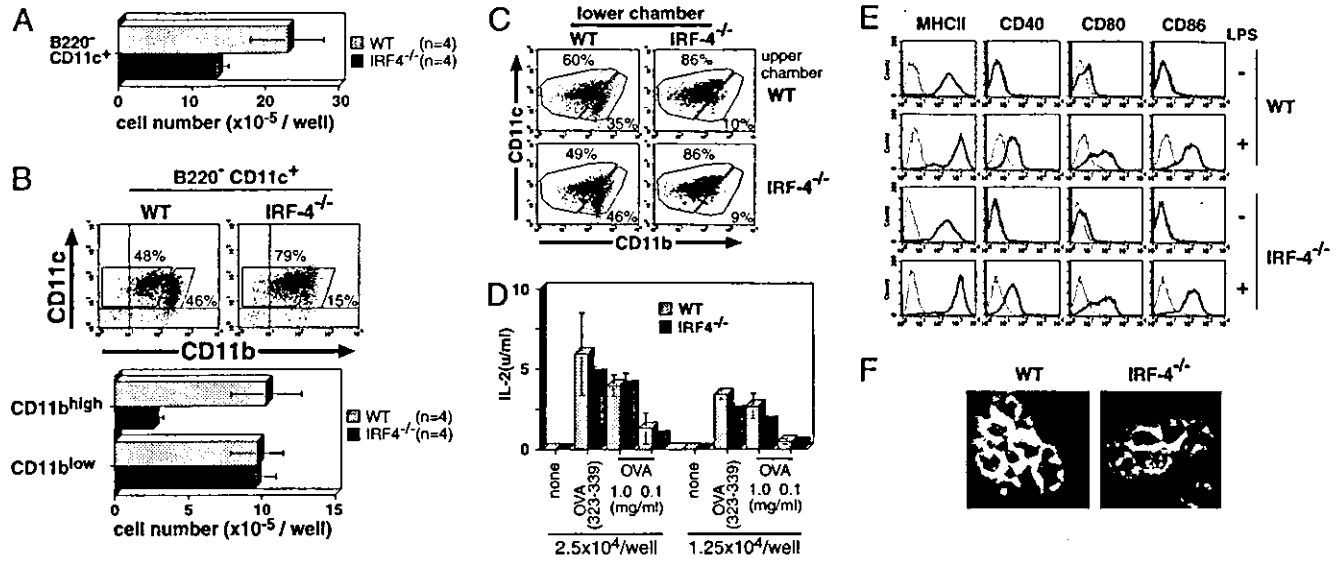

Fig. 2. Impaired development of the CD11b^{high} DC subset in the IRF-4$^{-/-}$ BM culture with Flt3L. Cells were stained with anti-CD11b-FITC, anti-CD11c-PE, and anti-B220-PerCP. (*A*) The number of B220^{-}CD11c^{+} cells from IRF-4$^{-/-}$ BM was compared with that from wild-type BM cells at 9 days after culture. (*B*) Analysis of the DC subsets in the Flt3L culture was performed, based on the expression of B220, CD11b, and CD11c. The values (%) indicate the proportion of each DC subset to B220^{-} cells (*Upper*). The number per well of CD11b^{low} and CD11b^{high} CD11c^{+} DCs from IRF-4$^{-/-}$ BM cells was compared with that from wild-type BM cells (*Lower*). (*C*) Soluble factors from BM cells stimulated by Flt3L were assessed by using transwell plates. BM cells at low density (5.2 × 10^{5} cells) were cultured in the lower chambers of transwell plates, separated by a 0.4-μm filter from BM cells at high density (5 × 10^{6} cells) in the upper chambers. Analysis of the DC subsets in the lower chambers was performed, based on the expression of CD11b and CD11c. (*D*) The antigen-presenting ability was examined as described in Fig. 1*E*. (*E*) The expression of MHC-II and costimulatory factors on DCs was analyzed by flow cytometry. (*F*) The morphology of LPS-stimulated DCs was observed by phase-contrast microscopy.

antigen presentation. The expression of CD40, CD80, and CD86 on CD11c^{+} cells from IRF-4$^{-/-}$ BM was similar to that of wild-type DCs. Strong up-regulation of the surface antigens was observed in wild-type DCs after stimulation with LPS. However, the up-regulation was not observed in most, if not all, CD11c^{+} cells from IRF-4$^{-/-}$ BM. Morphologically, the CD11c^{+} cells from IRF-4$^{-/-}$ BM did not develop the sheet-like veil structure after LPS stimulation (Fig. 1*G*). These results indicate that CD11c^{+} cells from IRF-4$^{-/-}$ BM fail to respond normally to LPS.

To determine whether the impaired DC development of CD11c^{+} cells from IRF-4$^{-/-}$ BM was caused by their intrinsic defects or environmental defects in the support of DC development in a GM-CSF-supplemented culture, we examined the generation of DCs from IRF-4$^{-/-}$ BM after a coculture with wild-type BM cells (Fig. 1*H*). The wild-type and IRF-4$^{-/-}$ BM could be distinguished by their expression of NPTII, whose gene was inserted when the IRF-4 gene was disrupted (23). Cells derived from IRF-4$^{-/-}$ BM cells (NPTII^{+}) in the mixed culture system did not express MHC-II at high levels, unlike those derived from wild-type BM (NPTII^{-}). This result indicates that the impaired DC development from IRF-4$^{-/-}$ BM cells is caused by cell autonomous defects.

To investigate the mechanisms underlying the impaired development of DCs from IRF-4$^{-/-}$ BM, we analyzed the mRNA expression of class II transactivator isoforms (CIITA types I and III), which are essential for the constitutive expression of MHC-II in DCs (37, 38) by an RT-PCR analysis. CD11c^{+} cells from IRF-4$^{-/-}$ BM expressed the CIITA type I and III mRNAs at almost negligible levels, as compared with the wild-type DCs (Fig. 1*I*), which might be responsible for the low-MHC-II expression level. CD11c^{+} cells from IRF-4$^{-/-}$ and wild-type BM expressed similar levels of the mRNAs encoding PU.1 and RelB, which are critical transcription factors for DC development (16, 17, 39, 40), the GM-CSF receptor components (α and cβ), and the M-CSF receptor, responsible for the interference of DC differentiation by M-CSF (41). Therefore, it is unlikely that the impaired DC development from IRF-4$^{-/-}$ BM cells is caused by the abnormal behaviors of PU.1 and RelB or abnormal responses to GM-CSF and M-CSF.

Defective Development Is Limited to CD11b^{high} DCs. We next used the Flt3L-supplemented BM culture system, which can give rise to B220^{-}CD11c^{+} conventional DCs and B220^{+}CD11c^{+} plasmacytoid DCs (42, 43). It is demonstrated that the conventional DCs from the culture contain two types of subsets, CD11b^{high} and CD11b^{low} DCs (10), and the plasmacytoid DCs do not express CD11b (42, 43). The number of B220^{-}CD11c^{+} conventional DCs developed from IRF-4$^{-/-}$ BM was reduced to ≈60% of that produced by wild-type BM (Fig. 2*A*). The number of B220^{+}CD11c^{+}CD11b^{-} plasmacytoid DCs that developed from IRF-4$^{-/-}$ BM, however, was similar to that from wild-type BM (Fig. 6, which is published as supporting information on the PNAS web site). We analyzed the expression of CD11b on B220^{-}CD11c^{+} cells from the Flt3L-supplemented BM culture. The proportion of CD11b^{high} cells to CD11c^{+} cells from the wild-type BM culture was 46%, whereas that from the IRF-4$^{-/-}$ BM was 15%. The absolute number of CD11c^{+}CD11b^{high} cells derived from IRF-4$^{-/-}$ BM was severely reduced, as compared with that from wild-type BM, whereas the absolute number of CD11c^{+}CD11b^{low} cells was unchanged (Fig. 2*B*). These results suggest that IRF-4 plays an important role in the development of CD11b^{high} conventional DCs, and is not essential for that of CD11b^{low} conventional DCs and plasmacytoid DCs in the Flt3L-supplemented BM culture. This defect of IRF-4$^{-/-}$ CD11b^{high} DCs could be due to the lack of soluble factor production by the IRF-4$^{-/-}$ BM cells. Therefore, we cultured IRF-4$^{-/-}$ and wild-type BM cells in the presence of Flt3L by using a transwell system as described (10). BM cells were cultured at low density in the lower chamber and at high density in the upper chamber in the presence of Flt3L (Fig. 2*C*). At the end of the culture, the generation of DCs in the lower chamber was analyzed by flow

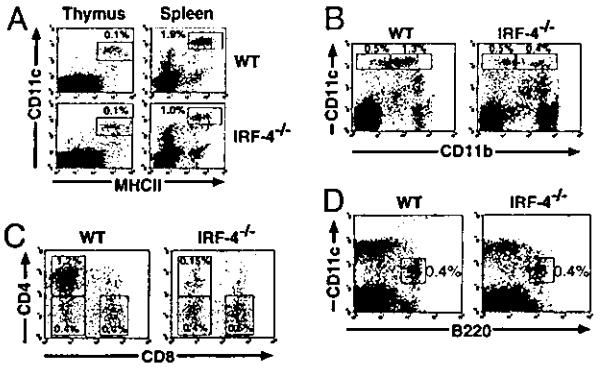

Fig. 3. Splenic CD11b^{high}CD4$^+$CD8α^- conventional DCs are selectively reduced in IRF-4$^{-/-}$ mice. Six-week-old male mice were used. (*A*) Thymic and splenic cells were stained with anti-MHC-II-FITC, anti-CD11c-PE, and anti-B220-PerCP. The CD11c^{high}MHC-II^{high} cells were analyzed after the B220$^+$ population was electrically gated out. (*B*) Splenic cells were stained with anti-CD11b-FITC, anti-CD11c-PE, and anti-B220-PerCP. Expression of CD11b on CD11c^{high} DCs was analyzed after the B220$^+$ population was electrically gated out. (*C*) Splenic cells were stained with anti-CD8α FITC, anti-CD11c-PE, and anti-CD4-CyChrome, and then the expression of CD4 and CD8α on CD11c^{high} DCs was analyzed. (*D*) Splenic cells were stained with anti-CD19-FITC and anti-NK1.1-FITC, anti-CD11c-PE, and anti-B220-biotin. The CD11c versus B220 profile is shown, after the CD19- or NK1.1-positive populations were electrically gated out to exclude B and NK cells. The biotinylated B220 antibody was detected with streptavidin-PerCP-Cy5.5. The values (%) indicate the proportion of gated populations to total thymic or splenic cells.

Table 1. Reduced number of CD4$^+$CD8$^-$ DCs in IRF-4$^{-/-}$ spleen

	Wild type	IRF-4$^{-/-}$
Splenocytes	1,040 ± 240	1,030 ± 190
CD11c^{high}MHC-II$^+$	22.5 ± 3.2	11.7 ± 3.1
CD11b^{high}CD4$^+$CD8$^-$	12.8 ± 2.1	1.5 ± 0.5
CD11b^{high}CD4$^-$CD8$^-$	4.6 ± 1.2	5.0 ± 1.3
CD11b^{low}CD4$^-$CD8$^+$	4.9 ± 1.0	5.1 ± 1.5
CD11c^{int}B220$^+$	5.1 ± 1.5	4.4 ± 0.5

Results represent the number of cells per spleen. Values are the means ± SD ($\times 10^{-5}$) of eight mice aged 6 weeks.

cytometry. In this system, the development of DCs from the wild-type BM cells in the lower chamber depended on the presence of wild-type BM cells at high density in the upper chamber (S.S. and A.K., unpublished data). Wild-type BM cells gave rise to a CD11c$^+$CD11b^{high} population when IRF-4$^{-/-}$ BM cells were cultured in the upper chamber (Fig. 2*C Lower Left*), suggesting that IRF-4$^{-/-}$ BM cells generated soluble factors that support DC development from the wild-type BM in the presence of Flt3L. On the contrary, the proportion of the CD11b^{high} population derived from IRF-4$^{-/-}$ BM cells remained low, even after they were cultured with wild-type BM in the upper chamber at high density (Fig. 2*C Upper Right*). Taken together, these results suggest that the defect in the generation of a CD11c$^+$CD11b^{high} population from IRF-4$^{-/-}$ BM in the presence of Flt3L is an intrinsic characteristic of these cells.

Next, we examined the properties of the CD11c$^+$ cells generated from IRF-4$^{-/-}$ BM in the Flt3L-supplemented culture. The CD11c$^+$ cells from IRF-4$^{-/-}$ BM were able to present whole OVA and its peptide (323–339 amino acid residues) to naive CD4$^+$ T cells from OT-II mice (Fig. 2*D*). They expressed MHC-II, CD40, CD80, and CD86 on the cell surface at levels similar to those of DCs from wild-type BM, before and after LPS stimulation (Fig. 2*E*). The CD11c$^+$ cells from IRF-4$^{-/-}$ and wild-type BM were morphologically indistinguishable (Fig. 2*F*). Because the majority of the IRF-4$^{-/-}$ DCs were CD11b^{low} conventional DCs (Figs. 2*B* and 6), these results suggest that the CD11b^{low} DCs in IRF-4$^{-/-}$ DCs are not impaired in their antigen-presenting function and responsiveness to LPS.

Defects of CD11b^{high} DCs in IRF-4$^{-/-}$ Spleen. Next, we examined the levels of conventional DCs *in vivo*. The majority of thymic and splenic conventional DCs belong to the CD11b^{low} and CD11b^{high} DC subsets, respectively (1). The proportion of conventional DCs in the thymus of IRF-4$^{-/-}$ mice was similar to that of the wild-type (0.1%), whereas it was reduced by ≈50% in the spleen (Fig. 3*A*). Among these DCs in the spleen, the proportion of CD11b^{high} DCs was markedly reduced, whereas that of CD11b^{low} DCs was not (Fig. 3*B*). Because the total splenic cell numbers were comparable (Table 1), the absolute number of CD11b^{high} DCs was selectively reduced in the IRF-4$^{-/-}$ spleen, consistent with the essential role of IRF-4 in the generation of CD11b^{high} DCs *in vitro*. Splenic CD11b^{high} DCs can be further subdivided into CD4$^+$CD8α^- and CD4$^-$CD8α^- subsets (6, 7). We further classified the splenic DCs, based on the expression of CD4 and CD8α. Flow cytometry analyses revealed that the CD4$^+$CD8α^- splenic DCs in IRF-4$^{-/-}$ mice were selectively reduced to ≈10% of the number in wild-type mice (Fig. 3*C*). As shown in Table 1, the absolute number of CD4$^+$CD8α^- DCs in the IRF-4$^{-/-}$ spleen was ≈10% of that found in the wild-type, resulting in the lower total number of CD11c^{high}MHC-II$^+$ DCs. These results demonstrated that the splenic CD11b^{high}CD4$^+$CD8α^- subset was selectively reduced among the conventional DCs in the IRF-4$^{-/-}$ mouse. We also examined the level of plasmacytoid DCs in the IRF-4$^{-/-}$ spleen. CD19$^+$and NK1.1$^+$ cells were gated out to exclude B cells and natural killer (NK) cells, which are B220$^+$ and CD11c^{low}, respectively (44). The proportion and the absolute number of CD11c^{int}B220$^+$ plasmacytoid DCs in IRF-4$^{-/-}$ spleen were not significantly different from those of the wild-type spleen (Fig. 3*D* and Table 1). Taken together, these results suggest that IRF-4 is critical for the development of the majority of CD11b^{high}CD4$^+$CD8α^- splenic conventional DCs, but not for that of CD11b^{high}CD4$^-$CD8α^- and CD11b^{low}CD4$^-$CD8α^+ splenic conventional DCs as well as plasmacytoid DCs.

IRF-4/IRF-8 Expression in Distinct DC Subsets. We next analyzed the expression of IRF-4 and IRF-8 in each splenic conventional DC subset at the single cell level, using four-color flow cytometry after triple staining of cell surface markers and intracellular IRFs (Fig. 4*A*). IRF-8 is another member of the IRF family that is important for DC development (25–28). In the wild-type spleen, all of the CD4$^+$CD8α^- DCs expressed IRF-4 and a small population (≈15%) expressed IRF-8, indicating that most of the CD4$^+$CD8α^- DCs express IRF-4 alone, and a minor population expresses both IRFs. In contrast, the majority of CD4$^-$CD8α^+ DCs in the wild-type spleen expressed IRF-8 and only ≈10% expressed IRF-4, indicating that most CD4$^-$CD8α^+ DCs express IRF-8, but not IRF-4. The majority of CD4$^-$CD8α^- splenic DCs expressed IRF-4 in wild-type mice, whereas ≈40% expressed IRF-8. In the IRF4$^{-/-}$ mouse spleen, all of the CD4$^-$CD8α^+ DCs expressed IRF-8, as expected. Interestingly, the small population of CD4$^+$CD8α^- DCs that remained in IRF4$^{-/-}$ mice expressed IRF-8, unlike the majority of these cells in wild-type mice. In addition, the majority of the CD4$^-$CD8α^- DCs, of which ≈60% did not express IRF-8 in wild-type mice, also expressed IRF-8 in the IRF-4$^{-/-}$ spleen. Taken together, these results indicate that the IRF-4 defect specifically affected the CD4$^+$CD8α^- and CD4$^-$CD8α^- DC subsets, which both preferentially expressed IRF-4 in wild-type mice.

The expression levels of IRF-4 and -8 in CD11c$^+$ cells from the BM culture with GM-CSF were analyzed by flow cytom-

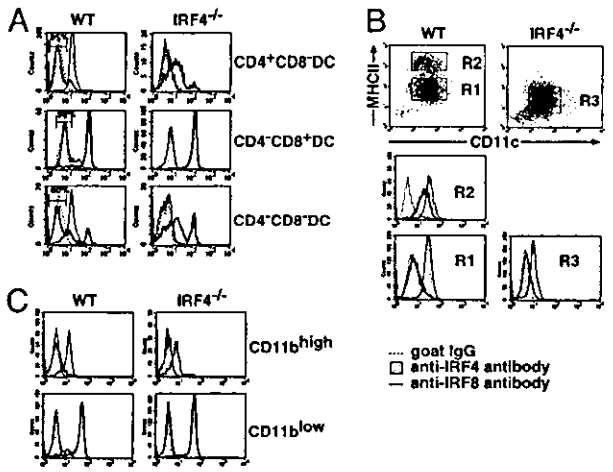

Fig. 4. IRF-4 and IRF-8 expression in various DC subsets. (*A*) Flow cytometric analysis of IRF-4 and IRF-8 expression in splenic conventional DCs. After low-density cells from wild-type and IRF-4$^{-/-}$ spleen were stained with anti-CD11c-PE, anti-CD4-allophycocyanin, and anti-CD8α-PerCP-Cy5.5, the cells were fixed, permeabilized, and stained with anti-IRF-4 or anti-IRF-8, followed by the Alexa Fluor 488-conjugated second antibody. CD11c^{high} DCs were gated on, and divided into the three subsets. Each subset was gated on, and IRF-4 and IRF-8 expression was examined. (*B*) Flow cytometric analysis of IRF-4 and IRF-8 expression in DCs from the GM-CSF culture. The wild-type and IRF-4$^{-/-}$ DCs were stained with anti-MHC-II-biotin and anti-CD11c-PE, followed by intracellular staining as described in *A*. (*C*) Flow cytometric analysis of IRF-4 and IRF-8 expression in DCs from the Flt3L culture. The wild-type and IRF-4$^{-/-}$ DCs were stained with anti-CD11b-biotin and anti-CD11c-PE, followed by intracellular staining as described in *A*. Cells were divided into CD11b^{high} and CD11b^{low} DCs as shown in Fig. 2*A*. Each population was gated on, and IRF-4 and IRF-8 expression was examined. The biotinylated antibodies used in *B* and *C* were detected with streptavidin-PerCP-Cy5.5.

etry (Fig. 4*B*). IRF-4 was expressed in both immature (R1) and mature (R2) wild-type DCs. However, IRF-8 was not expressed in immature wild-type DCs, suggesting a role of IRF-8 in the maturation of wild-type DCs, as reported (25–27), but not for their development in the GM-CSF-supplemented culture. The stimulation of the immature DCs with LPS induced IRF-8 expression, concomitant with their maturation (data not shown). In contrast, the majority of CD11c^{+} cells from IRF-4$^{-/-}$ BM (R3) expressed IRF-8. The aberrant expression of IRF-8 in these cells was insufficient to compensate for the lack of IRF-4, because these cells were unable to become functional DCs (Fig. 1).

We also analyzed the expression of IRF-4 and -8 in CD11b^{high} and CD11b^{low} DCs from the BM culture with Flt3L (Fig. 4*C*). The majority of CD11b^{high} cells from wild-type BM expressed IRF-4, but not IRF-8, whereas the majority CD11b^{low} cells expressed IRF-8, but not IRF-4. Interestingly, the majority of CD11b^{high} cells that were generated from IRF-4$^{-/-}$ BM expressed significant levels of IFR-8, unlike those derived from wild-type BM. This result is consistent to the *in vivo* observation that most CD11b^{high} splenic DCs express IRF-8 in the IRF-4$^{-/-}$ mouse (Fig. 4*A*).

Discussion

In the present study, we demonstrated that IRF-4 is important for most DCs of the CD11b^{high}CD8α^{-} subset, but not of the CD11b^{low}CD8α^{+} subset. We show that IRF-4 is expressed in most DCs of the CD11b^{high}CD8α^{-} subset, but not of CD11b^{low}CD8α^{+} subset in mouse spleen. The expression of IRF-4 in this DC subset was also confirmed in two BM culture systems. The DCs derived from BM in the presence of GM-CSF were uniformly CD11b^{high}, and most of them expressed IRF-4. Both CD11b^{high} and CD11b^{low} conventional DCs developed from BM in cultures supplemented with Flt3L; however, IRF-4 was preferentially expressed in the CD11b^{high} DC populations. Studies with mice lacking IRF-4 also determined that IRF-4 plays a critical role in these DC subsets. The development of CD11b^{high} DCs from IRF-4$^{-/-}$ BM *in vitro* was severely impaired in both culture systems. Furthermore, the number of CD4^{+}CD8α^{-} DCs, a major subset of CD11b^{high} DCs, was severely reduced in the spleen in mice lacking IRF-4. These results indicate that IRF-4 is selectively expressed in the CD11b^{high} subset of conventional DCs and plays critical roles in their development.

Comparative analyses of the expression of IRF-4 and IRF-8 in DCs revealed that conventional DCs can be grouped into three subpopulations: IRF-4(+)IRF-8(−), IRF-4(−)IRF-8(+), and IRF-4(+)IRF-8(+). The IRF-4(+)IRF-8(−) subpopulation preferentially belongs to the both CD11b^{high}CD4^{+} and CD11b^{high}CD4^{-} subsets, whereas the IRF-4(−)IRF-8(+) subpopulation preferentially belongs to the CD11b^{low}CD8^{-} DC subset. This observation may yield insight into the complicated developmental pathways of DCs. In mice lacking IRF-4, most of the DCs in CD11b^{high}CD8^{-} subset expressed IRF-8, although the majority of the DCs in this subset did not express IRF-8 in the wild-type mouse. These results suggest that a subset of IRF-8(−) DCs could not be generated in the absence of the IRF-4 gene, implying that IRF-4 is essential for the development of IRF-8(−), but not IRF-8(+), DCs. In contrast to the CD11b^{high} DC subsets, we did not detect any significant abnormality in the CD11b^{low}CD8α^{+} DCs in IRF-4$^{-/-}$ mice. This subpopulation of DCs in the spleens of wild-type and IRF-4$^{-/-}$ mice is IRF-8(+). The DCs that develop from the BM of IRF-4$^{-/-}$ mice in the Flt3L-supplemented culture are also IRF-8(+), suggesting that IRF-4 is not essential for the development and maturation of CD11b^{low}CD8α^{+} conventional DCs. Taken together, it is clear that all of the DC subsets that were examined expressed IRF-4 and/or IRF-8, suggesting the intriguing possibility that the function of either IRF-4 or IRF-8 is essential for the development of DCs.

The development of CD11b^{high} CD4^{+} DCs was severely impaired in mice lacking the RelB subunit of NF-κB (45). This defect in the DC subset is similar to the defects in IRF-4$^{-/-}$ mice. The expression of the IRF-4 gene is activated by c-Rel, another member of the NF-κB family, in B cells (46). RelB can bind to the same recognition DNA sequence as c-Rel in DCs (47). These findings suggest that IRF-4 might be regulated by RelB in DCs. In addition, tumor necrosis factor receptor-associated factor (TRAF) 6, which operates in the activation of NF-κB, is required for the development of conventional CD4^{+} DCs (45), suggesting that IRF-4 might also be regulated through TRAF6. The elucidation of the regulatory mechanisms for IRF-4 gene expression would help to clarify the developmental mechanisms of DCs.

Functional differences between CD11b^{high}CD8α^{-} and CD11b^{low}CD8α^{+} DCs have been suggested in a number of studies. These two subclasses of DCs regulate the development of T helper (Th) cells secreting discrete sets of lymphokines: CD11b^{high}CD8α^{-} DCs induce Th2-type responses and CD11b^{low}CD8α^{+} DCs induce Th1-type responses (48). The preferential induction of Th1 responses by CD11b^{low}CD8α^{+} DCs is mainly caused by their production of IL-12. In this study, we showed that IRF-4 and IRF-8 are expressed preferentially in CD11b^{high}CD8α^{-} and CD11b^{low}CD8α+ DCs, respectively. These IRFs may dictate not only the differentiation but also the function of these DC subsets. IRF-8 directs the expression of IL-12 (49) and IL-18 (50), promoting Th1-biased immune responses. On the other hand, IRF-4 is involved in the Th2-bias, by promoting IL-4 production by CD4^{+} T-cells and regulating their responsiveness to IL-4 (24, 51, 52). Therefore, it is intriguing to speculate that the IRF-4 expressed